Journal of
Marine Science and Engineering

MDPI

Article

The Intensification of Prolonged Cooling Climate-Exacerbated Late Ordovician–Early Silurian Mass Extinction: A Case Study from the Wufeng Formation–Longmaxi Formation in the Sichuan Basin

Zhibo Zhang [1], Yinghai Guo [1,*], Hengye Wei [2], Chunlin Zeng [3,4], Jiaming Zhang [1] and Difei Zhao [5,*]

[1] School of Resources and Geosciences, China University of Mining and Technology, Xuzhou 221116, China
[2] School of Earth Science and Technology, Southwest Petroleum University, Chengdu 610500, China
[3] Key Laboratory of Shale Gas Exploration, Ministry of Natural Resources, Chongqing Institute of Geology and Mineral Resources, Chongqing 401120, China
[4] National and Local Joint Engineering Research Center of Shale Gas Exploration and Development, Chongqing Institute of Geology and Mineral Resources, Chongqing 401120, China
[5] Geoscience and Unconventional Energy Research Center, Artificial Intelligence Research Institute, China University of Mining and Technology, Xuzhou 221116, China
* Correspondence: gyhai@163.com (Y.G.); difei.zhao@cumt.edu.cn (D.Z.)

Abstract: The Late Ordovician–Early Silurian period was a significant transitional phase in geological history and has garnered global interest. This study focuses on the black shale series of the Wufeng Formation–Longmaxi Formation of the Upper Ordovician–Lower Silurian period in the Sichuan Basin. Based on the logging curves and lithological characteristics of the Yucan-1 Well, 46 black shale samples were collected from the target layer section for clay mineral XRD (46 samples) analysis and whole-rock XRF (14 samples) analysis. The results indicate that three third-order sequences (SQ1, SQ2, and SQ3) are present in the Wufeng Formation–Longmaxi Formation of the Yucan-1 Well, and two subfacies and three microfacies were identified. In conjunction with the characteristics as well as the characteristic parameters of whole-rock oxide and clay mineral content ((I/C), (S + I/S)/(I + C), CIA, CIA-error, CIW, PIA, MAP, and LST), the Wufeng Formation–Longmaxi Formation of the Yucan-1 Well is divided into three intervals. Interval I is the Wufeng Formation. During this interval, weathering intensity, surface temperature, and precipitation gradually decreased, while the climate shifted from warm and humid to cold and dry. This corresponds to two pulse-type biological extinction events and represents an interval of increasing organic carbon burial. Interval II encompasses the bottom-middle part of the Longmaxi Formation. Weathering intensity, surface temperature, and precipitation were characterized by smooth, low values. Subsequently, the climate was predominantly cold and dry. This was the primary interval of organic carbon enrichment. Interval III extends from the upper part to the top of the Longmaxi Formation. Weathering intensity, surface temperature, and precipitation gradually increased. The climate transitioned from cold and dry to warm and humid. Organic carbon burial gradually decreased, while sea levels dropped. This indicates that climate cooling was the primary controlling factor for this biological extinction event. In combination with previous divisions of graptolite zones in the Yucan-1 Well, it is postulated that this biological extinction event may primarily have been pulse extinction. The continuous cooling of the climate in the later period led to the continuous extinction of organisms that survived the disaster. Until approximately 438.76 Ma at the top of the Longmaxi Formation, the climate environment recovered to pre-extinction conditions, with a transition to a warm and humid climate again.

Keywords: paleoclimate; Sichuan Basin; clay minerals; geochemistry; black shale; Late Ordovician–Early Silurian

Citation: Zhang, Z.; Guo, Y.; Wei, H.; Zeng, C.; Zhang, J.; Zhao, D. The Intensification of Prolonged Cooling Climate-Exacerbated Late Ordovician–Early Silurian Mass Extinction: A Case Study from the Wufeng Formation–Longmaxi Formation in the Sichuan Basin. *J. Mar. Sci. Eng.* **2023**, *11*, 1401. https://doi.org/10.3390/jmse11071401

Academic Editor: Assimina Antonarakou

Received: 12 June 2023
Revised: 3 July 2023
Accepted: 7 July 2023
Published: 11 July 2023

1. Introduction

The Late Ordovician–Early Silurian period was a unique period in geological history characterized by exceptional surface activity, including the convergence of extremely low glaciers, frequent global sea level fluctuations, active tectonic activity between plates, and localized volcanic eruptions. These major geological events led to revolutionary changes in the marine, continental, and atmospheric environments. Among them, the Hirnantian glaciation at the end of the Ordovician period witnessed the first mass extinction event in the Phanerozoic Eon. Nearly 85% of Earth's biological species became extinct, with its scale second only to the Permian–Triassic crisis [1–5]. There is ongoing debate regarding the relationship between this extinction event and the glaciation period. Some hypotheses include global cooling during the glaciation period leading to changes in the living environment of organisms and the subsequent extinction of those organisms [6,7] and the convergence of glaciers and sea level decline reducing the habitat of marine organisms [7]. The glaciation and mass extinction may also be related to global volcanic activity [8–12]. Other scholars believe that oceanic hypoxia [13,14], unique paleogeographic locations [15], or even the evolution of land plants [16,17] may have contributed to the extinction. All extinctions are inseparable from major changes in the atmosphere, biosphere, hydrosphere, and terrestrial environment. The fundamental cause of these environmental changes was intense volcanic activity in the Late Ordovician–Early Silurian period [13,15]. However, there is disagreement on how volcanic activity affects the environment [13]. Some scholars believe that volcanic activity leads to global warming, while others believe that it causes glacial movement. Nevertheless, volcanic activity is considered to be the main cause of mass extinction, and a dual-pulse extinction model has been established [18]. The latest high-resolution biodiversity curves [1,7,11] suggest that this extinction was persistent rather than a simple dual-pulse model and revisions have been made accordingly [12]. In addition, this extinction event resulted in the deposition of a set of black shales on a global scale, which has attracted widespread attention from scholars [19]. The deposition of these shales was controlled by multiple factors such as the primary productivity of the ancient ocean and the redox state of the seawater. These factors are intricately linked to this mass extinction event [19]. The degree of seawater circulation is related to the temperature gradient between the poles and the equator. This can explain the cold climate event because greenhouse climates are not conducive to the formation of temperature gradients, which, in turn, weaken seawater circulation. Conversely, a decrease in temperature promotes the formation of temperature gradients, leading to strong seawater circulation [20]. Therefore, Pohl et al. [21] used the fast ocean-atmosphere model (FOAM) to reconstruct the circulation patterns of the ocean surface water and the ocean-atmosphere during the Ordovician period. They found that the Hirnantian glaciation triggered an 11 °C temperature fluctuation, leading to strong seawater circulation. Paleocarbon dioxide content calculation models and biotic–abiotic indicator data [22–24] show that the atmospheric CO_2 content during this period was 14 to 22 times the current level. The glaciation that occurred during this period was characterized by high CO_2 contents [20,25,26]. During the Late Ordovician period, the South China region was located near the equator [27]. From the Late Ordovician to the Early Silurian period, the shallow carbonate platform of the Yangtze region in South China gradually evolved into a deep to shallow continental shelf, depositing a set of black shales [17,19]. Researchers have conducted extensive research on sedimentary facies [28], paleontology [29], and sedimentary environments [30], resolving a series of fundamental geological issues from the Late Ordovician–Early Silurian period in South China. At the end of the Late Ordovician period (Hirnantian phase), a brief glacial event in Gondwana caused a rapid decline in sea levels, accompanied by glacial deposits in high-latitude regions and shallow water deposits in low-latitude regions. The change in sea levels was significant, ranging from 50 to 100 m in Oslo, Norway [31], to 30 to 60 m on Anticosti Island in Quebec Province, Canada [32]. In addition, the change in sea levels was synchronous with that in the Yangtze region of southern China. Fluctuations in sea levels of approximately 20 m also occurred in southern China, along with the occurrence

of cold-water fauna in the Guanyinqiao member [33–35]. Therefore, the Yangtze region is considered an important window for studying the transitional period from the Late Ordovician to the Early Silurian period. Numerous studies have shown that a climate mutation occurred during the Late Ordovician period [36,37], leading to the expansion of ice caps on the Gondwana supercontinent and strong disturbances of carbon and nitrogen isotopes [38–41]. Despite profound research on global cooling caused by glaciation and hypoxia and the sulfidation of water bodies, there is a lack of in-depth research on the time scale of climate cooling caused by glaciation.

This research selects the shale of the Wufeng Formation–Longmaxi Formation of the Upper Ordovician (Katian phase) –Lower Silurian (Rhudanian phase) in the Yucan-1 Well of the Sichuan Basin as the research object. The climate during this period was studied by using the clay mineral content, type, and characteristic parameters (I/C and (S + I/S)/(I + C)) of the shale and the weathering index (CIA, CIW, PLA), surface temperature (LST), and surface rainfall (MAP) of major elements. This study aims to provide an explanation for the duration of the cooling (temperature drop) event associated with the glaciation and further enhance the understanding of the factors contributing to the Late Ordovician mass extinction (LOME) event.

2. Regional Geology

2.1. Geological Background

The study area is located in the northeastern part of Chongqing and belongs to the edge depression zone of the Daba Mountain platform on the Yangtze quasi-platform in terms of its tectonic position (Figure 1A). A series of fault-fold belts extending roughly parallel to the Chengkou fault are developed in the area. The Wufeng Formation–Longmaxi Formation is exposed between the Pingba Fault and the Shashi Concealed Fault. During the Late Ordovician–Early Silurian period, the study area was under the tectonic background of the passive continental margin of the northern edge of the Yangtze River [40], and was generally dominated by stable platform construction [19]. Affected by the rapid global sea level rise, the basin quickly changed from an oxidizing environment to a hypoxic environment. A series of black siliceous rocks, siliceous shales, carbonaceous shales, and carbonaceous siltstone shales of the Wufeng Formation -Longmaxi Formation is widely developed in the basin. Pyrite is developed and rich in graptolite shale. Multiple sets of spotted dolomites are commonly found in the Wufeng Formation, while the Longmaxi Formation contains a large number of caliche nodules and develops in layers. Between the black mud shales of the Wufeng Formation–Longmaxi Formation in the area, multiple sets of light gray, gray thin-layered, or lens-shaped muddy limestone, dolomitic sandstone, and fine-grained sandstone are developed. The fine-grained sandstone has developed parallel to the bedding and turns into brownish-yellow paleosols after severe weather. The total thickness of the Wufeng Formation–Longmaxi Formation mainly varies in an east–west direction (Figure 1B). Among them, the sedimentary thickness is the largest in the Tianba area, reaching more than 80 m. The thickness tends to decrease to both the east and west sides, even reducing to approximately 30 m [42].

2.2. Stratigraphic and Sedimentary Environment

The lithology of the Wufeng Formation–Longmaxi Formation in the Yucan-1 Well is mainly composed of carbonaceous shale, siliceous shale, siltstone shale, and siltstone. Li [43] divide44d the interval into eight graptolite zones based on graptolite fossils (Figure 2). According to the characteristics of the logging curve, the Wufeng Formation–Longmaxi Formation of the Yucan-1 Well is divided into two subfacies—deep-water continental shelf and shallow-water continental shelf—and four microfacies—deep-water cemented continental shelf, deep-water sandy continental shelf, shallow-water cemented continental shelf, and shallow-water sandy continental shelf [43]. Based on sedimentary facies, lithology, and logging characteristics, it is further divided into three third-order sequences (SQ1, SQ2, and SQ3) (Figure 2).

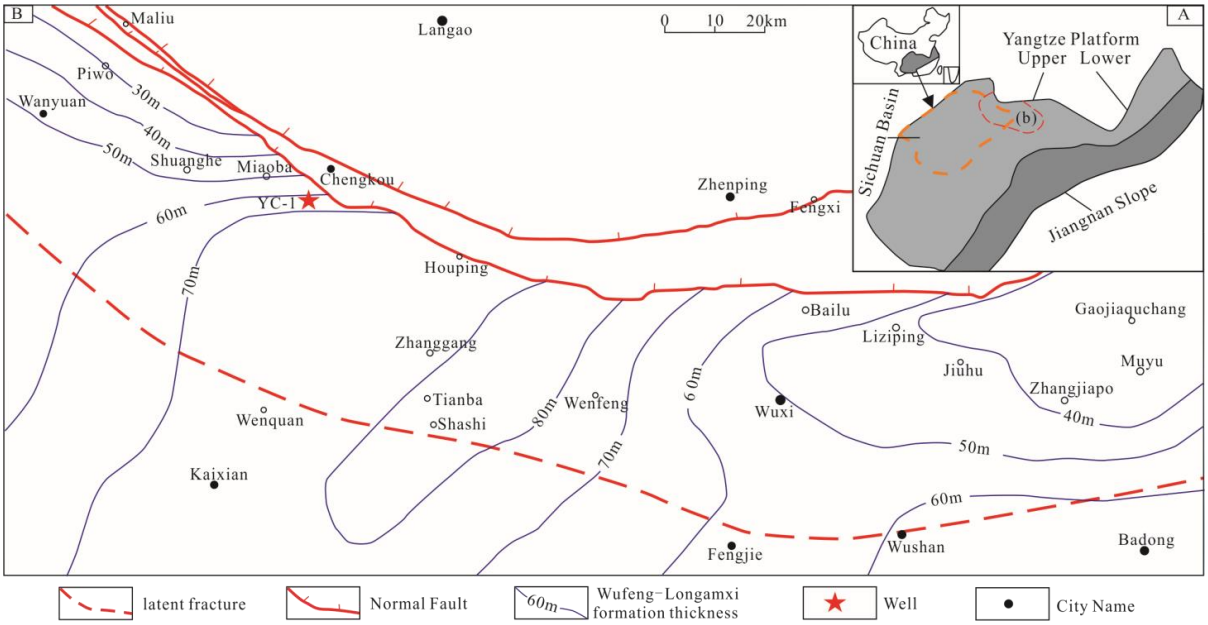

Figure 1. The study area and locations of profiles [19,42]. (**A**) Geological map of the Upper Yangzi region. (**B**) Shale thickness and sampling well locations of the Wufeng Formation-Longmaxi Formation in the study area.

(1) Sequence SQ1 corresponds to the Wufeng Formation and developed the transgressive systems tract (TST). The TST was mainly composed of gray-black siliceous shale (Figure 2a) and supplied black carbonaceous shale (Figure 2b). In the TST, the sea level rose, the available space increased, and the input of detritus became insufficient. The process of increasing the mud content upwards formed a set of fine-grained deposits dominated by black mudstone, black carbonaceous shale, and black siliceous rock. Horizontal bedding was developed on shale (Figure 2b), and graptolite-rich shale can be observed in the Wufeng Formation (Figure 2a), corresponding to the deep-water cemented continental shelf microfacies. The thin mudstone at the top of the Wufeng Formation is the regressive systems tract (RST) (Figure 2), which corresponds to the global ice epoch event with the lowest sea level.

(2) Sequence SQ2 corresponds to the bottom-middle part of the Longmaxi Formation (depth 1204–1160 m). From 1204 to 1192 m is the TST, corresponding to the deep-water cemented continental shelf microfacies. The sea level rose, the available space increased, and the supply of detritus became insufficient. The TST process was a rise in the mud content. From 1192 to 1160 m was the RST, corresponding to the deep-water sandy continental shelf and deep-water cemented continental shelf microfacies. The RST reflects the decline in sea levels, reduction in available space, increase in detritus supply, and process of decreasing mud content and increasing sand content upwards (Figure 2). The lithology is composed of carbonaceous shale, siliceous carbonaceous shale, carbonaceous siltstone sandstone, and carbonaceous shale. Calcareous nodules can be observed (Figure 2c).

(3) Sequence SQ3 corresponds to the middle-upper part of the Longmaxi Formation (depth 1160–1080 m) and developed a TST and RST (1160–1080 m). Among them, the lithologies of the 1160–1146 m section are composed of siltstone cemented rock, carbonaceous mud shale (Figure 2d), siltstone shale, carbonaceous siltstone sandstone, and muddy siltstone sandstone. The siltstone shale developed horizontal bedding (Figure 2e). The TST corresponds to the deep water sandy continental shelf, reflecting the rising sea level, increasing available space, and insufficient debris supply. The RST developed two subfacies—deep-water continental shelf subfacies and shallow-water continental shelf subfacies—and four microfacies—deep-water cemented continental

shelf, deep-water sandy continental shelf, shallow-water cemented continental shelf, and shallow-water sandy continental shelf microfacies (Figure 2). The natural gamma value increases from bottom to top, reflecting a decrease in mud content from bottom to top. The sea level decreased and the supply of terrestrial detritus filled the accommodation space.

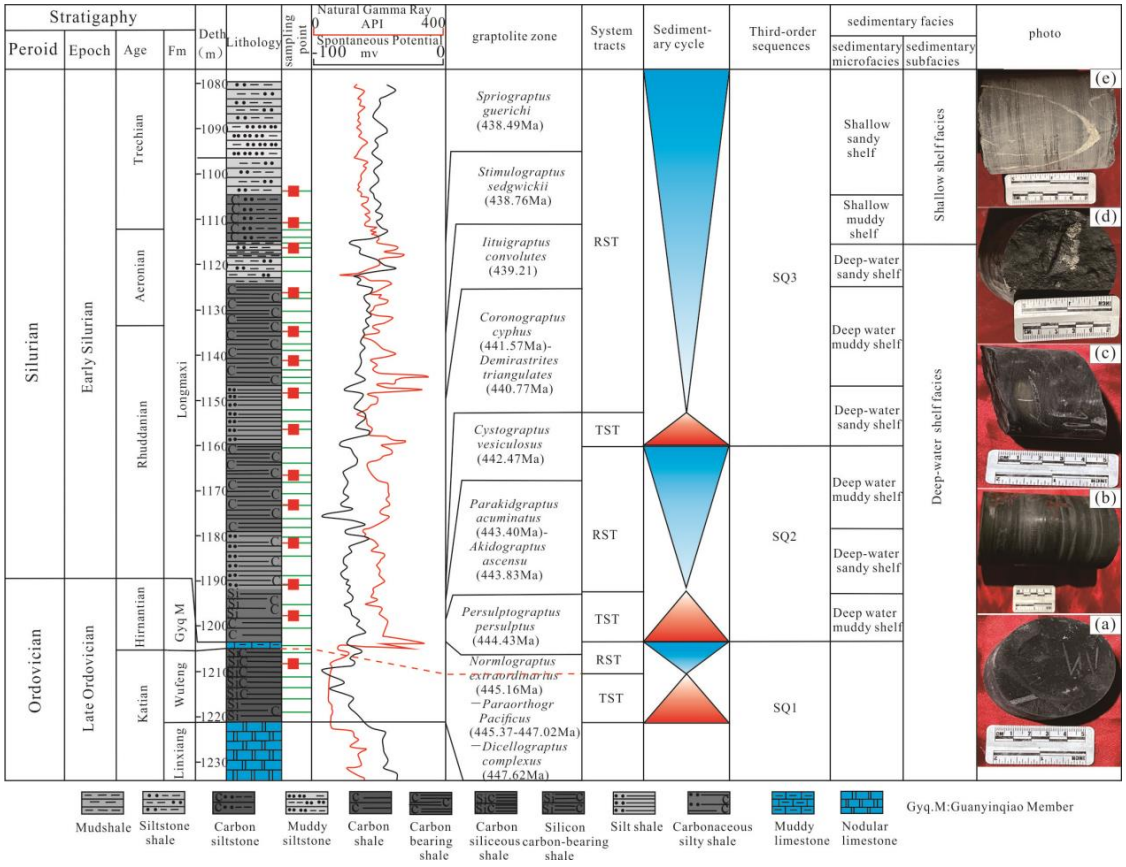

Figure 2. Lithostratigraphic column and sampling location of the Yucan-1 Well [43]. (**a**) Gray-black siliceous shale. (**b**) Horizontal shale. (**c**) Carbonaceous shale with calcareous nodules. (**d**) carbonaceous mud shale. (**e**) Siltstone shale with horizontal bedding.

3. Materials and Methodology

3.1. Materials

Forty-six shale samples were collected from the Wufeng Formation–Longmaxi Formation of the Yucan-1 Well in the Chengkou area of Chongqing City (Figure 2). Based on the vertical changes of lithology, 14 shale samples were selected for major element testing (Figure 2, red square), and all shale samples were selected for clay minerals (Figure 2, green line).

3.2. Methodology

Sample pre-treatment: Fresh drilling core samples were collected and crushed in the pre-treatment room. The samples were ground into powder using an electromagnetic sample crusher (DF-4), sieved through a 200-mesh sieve, packed into sample bags, sealed, and tested. Major elements and clay minerals were analyzed and tested at the Chongqing Mineral Resources Supervision and Testing Center of the Ministry of Natural Resources.

(1) Whole-rock major element testing

A ZSX Primus II wavelength dispersive X-ray fluorescence spectrometer (XRF) produced by Rigaku of Japan was used with a 4.0 kW end-window rhodium target X-ray tube.

The test conditions were 50 kV voltage and 60 mA current. The analysis lines for major elements were all Kα. The standard curve was established using the national standard substance rock series GBW07101-14, soil series GSS07401-08, and water and sediment series GBW07302-12. Data correction was performed using the theoretical α coefficient method. The relative standard deviation (RSD) of the test was <2%.

(2) Whole-rock TOC testing

A total of 100 mg of the sample ground using a 200-mesh sieve was weighed and placed in a centrifuge tube. A total of 4 mol/L HCl was added and shaken to combine. After soaking and dissolving for 24 h, the tube was centrifuged and the supernatant was poured off. Deionized water was added and centrifuged again. This process was repeated three times. After the pH of the supernatant was found to be neutral using pH test paper, the sample was dried in a freeze dryer for 48 h. A total of 30 mg of the dried sample was weighed, wrapped in tin foil, folded and compacted, and placed in a MAT-253 elemental analyzer–isotope ratio mass spectrometer for testing. The analysis error was less than 0.2‰.

(3) Whole-rock clay mineral testing

X-ray diffraction analysis (XRD) was used to determine the type and relative content of clay minerals in the sample. The sample was extracted using the sedimentation method. After crushing the sample to a particle size of <0.2 mm, it was soaked in distilled water for more than 48 h. The clay mineral suspension was drawn off and the resulting clay minerals were made into natural oriented slices (N slices), ethylene glycol saturated slices (EG slices), and high-temperature slices (T slices) and treated by heating (550°/2 h) for experimental analysis. The measuring instrument was a Panaco X'pert diffractometer from the Netherlands: Cu target radiation, X-ray tube working voltage of 40 kV, current of 40 mA, RS = 5.5 mm, scanning angle (2θ) range of 3~30°, scanning speed of 10°/min. Different clay minerals have specific layer shapes and interlayer substances, resulting in different basal spacing (d) and basal diffraction intensities of clay minerals [44]. For example, the d (001) of the chlorite group is 1.41~1.435 nm, the d (001) of illite is 0.995~1.00 nm, and the basal spacing of the montmorillonite group varies greatly (1.2~1.6 nm) [44]. Only after treatment with ethylene glycol can the d (001) of montmorillonite expand to 1.7 nm [44]. Therefore, the type of clay mineral can be determined based on the difference in basal spacing (d (001)) and basal diffraction intensity [44]. The weight coefficients commonly used are those of Johns et al. [45] and Biscaye [46]. The weight peak intensity standards they used are as follows: the intensity of the 1.7 nm diffraction peak treated with ethylene glycol multiplied by 1 is the weight peak intensity of montmorillonite; the intensity of the 1.0 nm diffraction peak multiplied by 4 is the weight peak intensity of illite; and the intensity of the 0.7 nm diffraction peak multiplied by 2 is the weight peak intensity of kaolinite plus chlorite. The content ratio between kaolinite and chlorite can be directly calculated from the ratio of the intensities of the 0.353 nm diffraction peak (chlorite) and the 0.356~0.358 nm diffraction peak (kaolinite) [45,46]. Illite crystallinity was measured using the Kübler index, using Jade software to measure the half-height width of the Illite d (001) diffraction peak [47,48].

3.3. Index Reliability Evaluation

(1) Chemical Index of Alteration (CIA)

The chemical index of alteration (CIA) indicates the degree of chemical weathering of soils and sediments and can be used for paleoclimate reconstruction [49]. During the chemical weathering process, as the climate becomes warmer and more humid, the reduction of free cations produces higher CIA values. The formula is as follows:

$$CIA = [Al_2O_3/(Al_2O_3 + CaO^* + Na_2O + K_2O)] \times 100 \quad (1)$$

where all oxides are expressed in moles, and CaO* represents the CaO in the silicate component. The correction steps for CaO* followed the method of McLennan [50]: Use P_2O_5 data to correct for CaO in apatite ($CaO = CaO - 10/3 \times P_2O_5$). If CaO is greater than

Na_2O, then CaO* is equal to Na_2O; if CaO is less than Na_2O, then CaO* is equal to CaO. The characteristic of unweathered bedrock is a low CIA value (45–55), which approaches 100 as weathering progresses and mobile elements are lost. The K_2O content of rocks can be affected by the alteration of potassium elements, and this secondary sedimentation process can result in potassium ions being absorbed by burial fluids in severely altered rocks [49]. The CIA value can be corrected using the method of Panahi et al. [51].

$$K_2Ocorr = [mAl_2O_3 + m(CaO^* + Na_2O)]/(1-m) \quad (2)$$

$$m = K_2O/(Al_2O_3 + CaO^* + Na_2O + K_2O) \quad (3)$$

By replacing K_2O in Equation (1) with K_2Ocorr, the corrected CIA (CIAcorr) can be calculated. When CIAcorr < CIA, CIA can more accurately reflect the weathering intensity; otherwise, CIAcorr has higher credibility.

The land surface temperature (LST) can be calculated using the formula of Yang et al. [52]:

$$LST = 0.56 \times CIA - 25.7 \quad (4)$$

where LST is in °C and the standard error (SE) = ±8.66 °C. When CIA is between 50 and 90, this formula is reliable (corresponding to −3.83~26.35 °C). A three-point moving average is used to smooth the LST record to reflect the time-averaged conditions at each point while taking into account the variability of the sampling resolution [52].

(2) Chemical Weathering Index (CIW)

Since excessive K_2O is frequently found in sedimentary rock units [49], the CIA value is greatly affected by the alteration of potassium elements. Harnois [53] proposed an alternative index, the chemical weathering index (CIW), which is based on the same principle as CIA but removes K_2O. The formula is as follows:

$$CIW = [Al_2O_3/(Al_2O_3 + CaO^* + Na_2O)] \times 100 \quad (5)$$

Sheldon et al. [54] proposed the relationship between CIW and the mean annual precipitation (MAP) as follows:

$$MAP(mm/yr) = 221.12e^{0.0197(CIW)} \ (SE = \pm 1.01 \text{ mm}) \quad (6)$$

CIW is not suitable for samples with a high K content as the research object [53,55]. Due to the large magnitude of K, its removal not only results in insignificant numerical changes but also leads to higher values. Therefore, many scholars prefer to use CIA to indicate the degree of rock weathering. However, variations in individual components of CIA, such as K, can affect the results. Additionally, the content of Al can be altered by chemical deposition. Consequently, CIA may not be applicable to all sedimentary environments [56]. To mitigate the influence of diagenesis and later diagenetic processes on estimating the degree of chemical weathering, Fedo et al. [57] proposed the use of the plagioclase alteration index (PIA), which can also be employed to correct for plagioclase weathering [57]. The expression for PIA is as follows:

$$PIA = [(A1_2O_3\text{-}K_2O)/(Al_20_3 + CaO^* + Na_2O\text{-}K_2O)] \times 100 \quad (7)$$

In conclusion, by calibrating the CIA, CIW, and PIA parameters, the results presented in Table 1 were obtained. Furthermore, using the calibrated CIA and CIW values, parameters for land surface temperature (LST) and mean annual precipitation (MAP) were calculated. These results are considered reliable and can be utilized to reflect the variations in paleoclimate, paleotemperature, and precipitation during the Late Ordovician to Early Silurian period.

Table 1. Major elements and their characteristic ratios of Yucan-1 Well in the study area.

Sample	F m	Depth	TiO_2	FeO	Fe_2O_3	Na_2O	MgO	SiO_2	K_2O	CaO	P_2O_5	Al_2O_3	CIA-Error	CIA	CIW	PIA	LST	MAP/mm/yr
YC1-1	Long maxi	1105.80	0.64	3.27	2.37	1.16	2.29	66.65	3.41	0.64	0.24	9.24	68.94	67.69	90.23	85.36	12.21	227.40
YC1-5		1109.38	0.51	1.17	3.23	0.95	1.18	74.82	2.12	0.39	0.20	9.34	77.83	76.98	93.28	91.47	17.41	224.31
YC1-14		1116.54	0.58	1.56	3.33	1.19	1.89	62.16	2.94	2.51	0.28	3.41	41.67	39.06	58.89	16.49	−3.83	225.50
YC1-24		1126.10	0.60	1.58	4.18	0.95	1.97	61.09	3.38	1.02	0.28	3.11	45.04	41.32	75.00	−35.22	−2.56	225.36
YC1-35		1135.30	0.59	1.48	3.71	1.13	1.93	63.02	3.38	0.81	0.23	3.22	44.28	41.42	73.29	−15.79	−2.50	226.51
YC1-44		1141.39	0.49	0.84	4.1	1.06	1.58	68.72	2.64	1.25	0.22	9.27	69.60	68.73	85.46	80.79	12.79	224.75
YC1-54		1148.10	0.45	1.54	2.76	0.84	4.43	56.23	2.455	6.31	0.20	3.18	52.87	43.47	65.43	30.15	−1.36	226.90
YC1-63		1156.65	0.27	0.47	2.52	0.52	0.76	78.51	1.37	1.38	0.19	8.43	78.59	77.77	89.02	87.16	17.85	226.87
YC1-74		1166.10	0.38	0.45	3.93	1.00	0.91	69.79	2.00	1.09	0.28	9.18	75.42	74.41	88.81	86.13	15.97	225.71
YC1-84		1173.84	0.29	0.64	3.48	0.67	9.71	41.87	1.513	12.17	0.29	4.58	71.18	61.62	77.36	69.59	8.81	226.38
YC1-94		1182.51	0.24	0.74	2.07	0.78	0.67	81.06	1.2	1.03	0.19	6.32	73.46	72.67	84.30	81.31	15.00	227.01
YC1-104		1190.52	0.25	1.13	1.69	0.62	0.79	77.99	1.32	0.98	0.20	8.43	79.56	78.91	90.03	88.40	18.49	226.87
YC1-114		1198.27	0.14	1.54	1.05	0.35	0.78	88.67	0.72	1.1	0.10	5.54	80.49	79.60	88.78	87.32	18.87	227.82
YC1-126	Wufeng	1209.13	0.15	2.41	1.04	0.27	0.59	87.65	0.62	0.83	0.11	15.29	93.07	92.95	96.59	96.45	26.35	222.12

4. Result

4.1. TOC and Major Elements Characteristics

The TOC content of the Wufeng Formation in the Yucan-1 Well ranges from 1.01 to 3.15%, with an average value of 1.85% (Table 1, Figure 3a). The TOC content of the Longmaxi Formation ranges from 0.24 to 6.11, with an average value of 3.42% (Table 1, Figure 3b). In the Wufeng Formation, the TiO_2 content is 0.15%, FeO is 2.41%, Fe_2O_3 is 1.04%, Na_2O is 0.27%, MgO is 0.59%, SiO_2 is 87.65%, K_2O is 0.62%, CaO is 0.83%, P_2O_5 is 0.11%, and Al_2O_3 is 15.29% (Figure 3a). The range of TiO_2 in the Longmaxi Formation is between 0.14 and 0.64%, with an average value of 0.30; the range of FeO is between 0.14 and 0.64%, with an average value of 1.79%; the range of Fe_2O_3 is between 1.04 and 4.18%, with an average value of 2.06%; the range of Na_2O is between 0.27 and 1.19%, with an average value of 0.60%; the range of MgO is between 0.59 and 9.71%, with an average value of 2.79%; the range of SiO_2 is between 41.87 and 88.67%, with an average value of 75.07%; the range of K_2O is between 0.62 and 3.41%, with an average value of 1.53%; the range of CaO is between 0.39 and 12.17%, with an average value of 3.37%; the range of P_2O_5 is between 0.10 and 0.29%, with an average value of 0.16%; and the range of Al_2O_3 is between 3.11 and 15.29%, with an average value of 7.94% (Figure 3b). Overall, it can be observed that both the Wuying and the Longmaxi Formations have high characteristics of silicon, iron, calcium, potassium, and aluminum and low characteristics of phosphorus, sodium, and titanium (Figure 3).

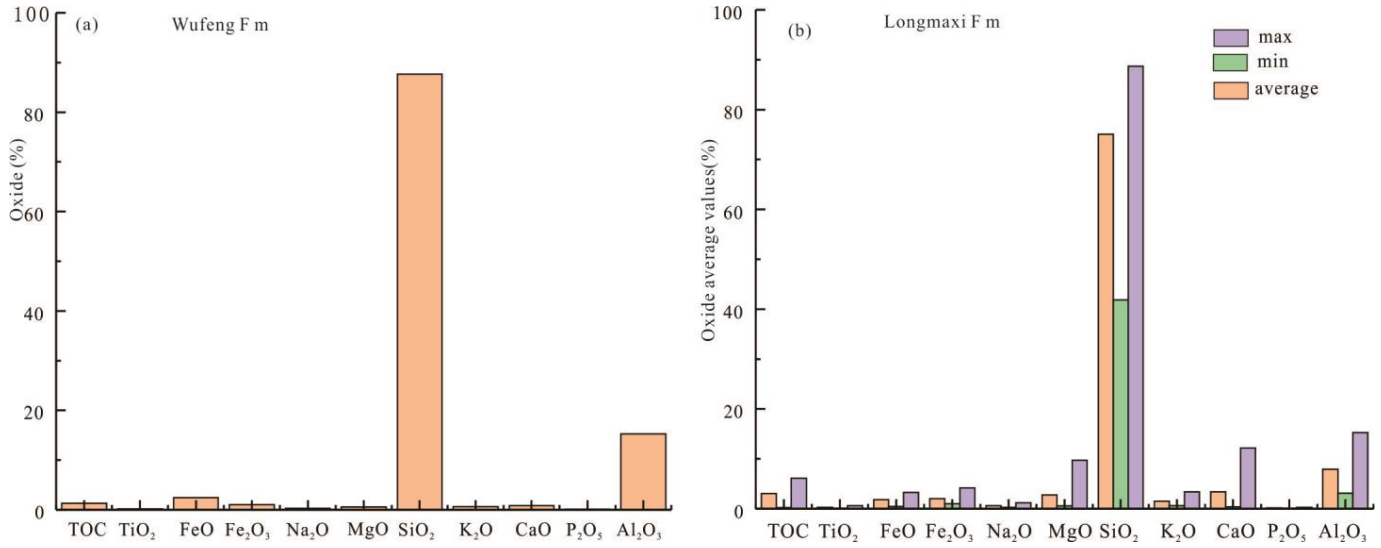

Figure 3. Histogram of the content of TOC and oxides in the Wufeng Formation–Longmaxi Formation of the Yucan-1 Well. (**a**) Histogram of TOC and major elements in the shale of the Wufeng Formation. (**b**) Histogram of TOC and major elements in the shale of the Longamxi Formation.

4.2. Chemical Weathering Index Characteristics

In the Wufeng Formation, the CIA-error content is 93.07, CIA is 92.95, CAW is 96.59, PIA is 96.45, LST is 26.35 °C, and MAP is 222.12 mm/yr (Table 1). In the Longmaxi Formation, the range of CIA-error is between 41.67 and 80.49, with an average value of 66.07; the range of CIA is between 39.06 and 79.60, with an average value of 63.36; the range of CIW is between 58.89 and 93.28, with an average value of 81.53; the range of PIA is between −35.22 and 91.47, with an average value of 57.94; the range of LST is between −3.83 and 18.87 °C, with an average value of 9.38 °C; the range of MAP is between 224.31 and 227.82 mm/yr, with an average value of 226.26 mm/yr (Table 1). Overall, the CIA-error, CIA, CIW, PIA, MAP, and LST of the Wufeng and Longmaxi Formations can be observed to be negatively correlated with LST.

4.3. Clay Mineralogy Content Characteristics

The kaolinite (K) content of the clay minerals in the Wufeng Formation ranges from 1.00 to 3.00%, with an average value of 1.67%. The chlorite (C) content ranges from 2.00 to 3.00%, with an average value of 2.83%. The illite (I) content ranges from 7.00 to 18.00%, with an average value of 10.14%. The crystallinity varies from 0.43° to 0.54°, with an average value of 0.48. The illite/montmorillonite interlayer (I/S) content ranges from 63.00 to 84.00%, with an average value of 78.14%. The chlorite/montmorillonite mixed layer (C/S) content ranges from 4.00 to 22.00%, with an average value of 9.17%. The illite/montmorillonite interlayer (I/S) content in the mixed layer ratio ranges from 5.00 to 8.00%, with an average value of 6.86%. The chlorite/montmorillonite mixed layer (C/S) content in the mixed layer ratio ranges from 14.00 to 17.00%, with an average value of 15.33% (Table 2, Figure 4a). The kaolinite (K) content of clay minerals in the Longmaxi Formation ranges from 1.00 to 3.00%, with an average value of 1.75%. The chlorite (C) content ranges from 1.00 to 9.00%, with an average value of 2.72%. The illite (I) content ranges from 5.00 to 22.00%, with an average value of 9.23%. The crystallinity varies from 0.42° to 0.63°, with an average value of 0.53°. The illite/montmorillonite interlayer (I/S) content ranges from 57.00 to 95.00%, with an average value of 87.00%. The chlorite/montmorillonite mixed layer (C/S) content ranges from 1.00 to 9.00%, with an average value of 3.85%. The illite/montmorillonite interlayer (I/S) content in the mixed layer ratio ranges from 6.00 to 9.00 %, with an average value of 7.64%. The chlorite/montmorillonite mixed layer (C/S) content in the mixed layer ratio ranges from 10.00 to 24.00%, with an average value of 15.25% (Table 2, Figure 4b). In summary, both the Wuying and Longmaxi Formations are dominated by illite/montmorillonite interlayer (I/S) minerals, followed by illite, chlorite, and kaolinite.

Table 2. Clay mineral content and characteristic ratios of Yucan-1 Well in the study area.

F m	Sample	Depth	TOC	Clay Mineral Content (%)						Mixed-Layer Ratio (S%)	
				K	C	I	S	I/S	C/S	I/S	C/S
Longmaxi	YC1-1	1105.80	0.24	3	5	13	/	74	5	6	17
	YC1-5	1109.38	2.03	2	4	11	/	79	4	6	21
	YC1-7	1110.90	0.50	3	9	22	/	57	9	6	12
	YC1-9	1112.30	2.37	1	4	14	/	76	5	7	12
	YC1-12	1115.00	1.72	3	5	15	/	68	9	6	14
	YC1-14	1116.54	2.10	1	3	8	/	82	6	7	12
	YC1-17	1119.36	2.14	2	4	13	/	76	5	8	16
	YC1-19	1121.00	0.95	2	1	8	/	84	5	8	11
	YC1-24	1126.10	2.09	/	/	13	/	87	/	9	/
	YC1-26	1127.50	3.05	1	2	9	/	86	2	8	11
	YC1-29	1130.05	3.65	1	2	7	/	88	2	6	15
	YC1-32	1133.10	3.98	1	2	10	/	85	2	8	24
	YC1-35	1135.30	3.62	/	1	9	/	88	2	8	20
	YC1-39	1138.00	2.79	1	2	11	/	83	3	9	11
	YC1-41	1139.60	4.09	/	1	7	/	89	3	9	17
	YC1-44	1141.39	3.31	/	1	7	/	89	3	7	10
	YC1-47	1142.80	4.00	/	1	10	/	88	1	8	12
	YC1-49	1144.20	2.78	/	/	9	/	89	2	7	19
	YC1-52	1146.60	2.64	/	1	11	/	86	2	7	14
	YC1-54	1148.10	3.17	/	/	6	/	93	1	8	15
	YC1-58	1151.50	2.90	/	/	5	/	95	/	9	/
	YC1-61	1154.60	2.96	/	/	7	/	93	/	8	/
	YC1-63	1156.65	3.41	/	/	7	/	93	/	9	/
	YC1-68	1160.36	3.33	/	/	7	/	93	/	8	/
	YC1-72	1164.03	5.97	/	/	8	/	92	/	8	/
	YC1-74	1166.10	4.64	/	/	11	/	89	/	6	/

Table 2. *Cont.*

F m	Sample	Depth	TOC	Clay Mineral Content (%)						Mixed-Layer Ratio (S%)	
				K	C	I	S	I/S	C/S	I/S	C/S
Wufeng	YC1-78	1168.70	4.26	/	/	7	/	93	/	6	/
	YC1-81	1171.35	4.90	/	/	6	/	94	/	8	/
	YC1-84	1173.84	6.11	/	/	6	/	94	/	9	/
	YC1-86	1176.16	5.31	/	/	7	/	93	/	7	/
	YC1-89	1179.05	3.97	/	/	6	/	94	/	9	/
	YC1-92	1181.40	5.13	/	/	8	/	92	/	9	/
	YC1-94	1182.51	3.26	/	/	17	/	83	/	7	/
	YC1-96	1184.59	4.87	/	/	6	/	94	/	9	/
	YC1-102	1189.10	3.02	/	/	9	/	91	/	7	/
	YC1-104	1190.52	4.74	/	/	8	/	92	/	8	/
	YC1-109	1195.13	4.38	/	/	8	/	92	/	7	/
	YC1-114	1198.27	4.36	/	1	7	/	86	6	9	22
	YC1-118	1201.20	4.69	/	/	7	/	93	/	7	/
	YC1-121	1204.00	3.15	1	2	8	/	83	6	7	16
	YC1-123	1206.70	2.70	2	3	10	/	63	22	7	17
	YC1-126	1209.13	1.30	1	3	12	/	75	9	5	15
	YC1-128	1211.07	1.01	/	/	18	/	82	/	6	/
	YC1-132	1214.95	1.47	2	3	7	/	81	7	7	16
	YC1-134	1217.00	2.18	1	3	8	/	84	4	8	14
	YC1-136	1219.00	1.12	3	3	8	/	79	7	8	14

Notes: K = Kaolinite; C = Chlorite; S = Smectite; I = Illite; I/S = Illite/Smectite mixed layer; % S of S in %S-I/S.

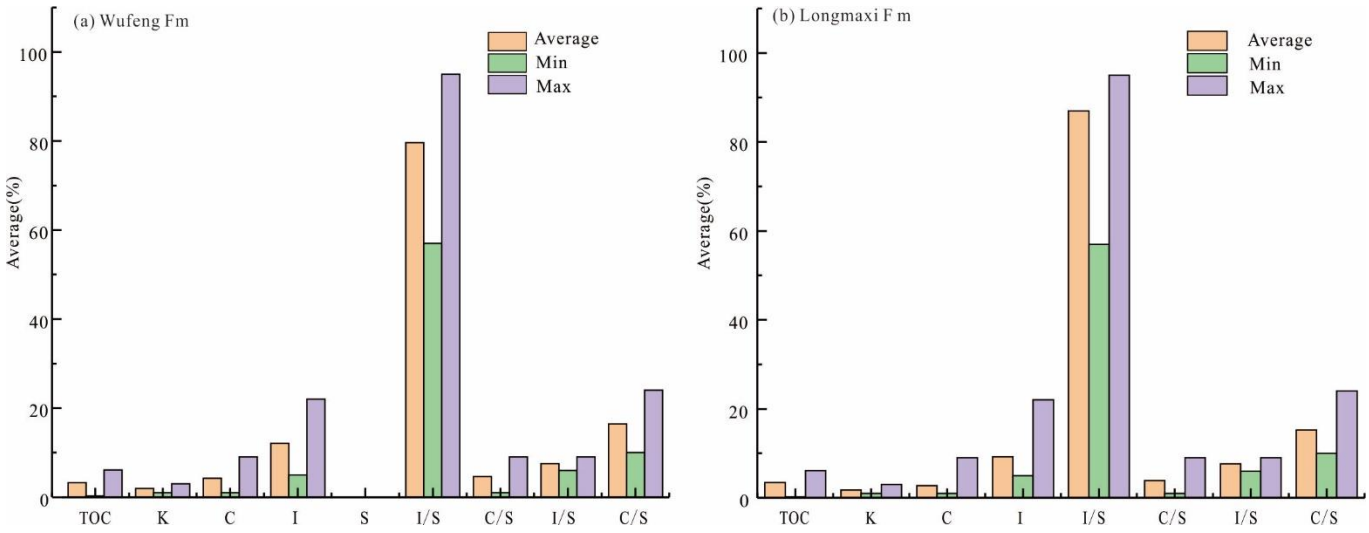

Figure 4. Histogram of the content of black TOC and shale clay minerals in the Wufeng Formation–Longmaxi Formation. (**a**) Histogram of clay mineral content in the shale of the Wufeng Formation. (**b**) Histogram of clay mineral content in the shale of the Longmaxi Formation.

TOC is relatively low in the Wufeng Formation and increases in the Longmaxi Formation, with a decreasing trend towards the top of the muddy limestone. The kaolinite, chlorite, and chlorite/montmorillonite mixed layer show an increasing–decreasing trend from the bottom of the Wufeng Formation–Longmaxi Formation to the middle of the Longmaxi Formation, where none of these three minerals are present. Towards the top of the Longmaxi Formation, there is an increasing-decreasing trend (Figure 5). Illite shows an overall increasing-decreasing-increasing–decreasing trend in the Wuying–Longmaxi Formation (Figure 5). The illite/montmorillonite mixed layer shows an overall decreasing–increasing–decreasing–increasing trend in the Wufeng Formation–Longmaxi Formation (Figure 4). In summary, it was found that the kaolinite, chlorite, illite, and chlorite/montmorillonite mixed layer have a positive correlation with each other and a negative correlation with the

illite/montmorillonite mixed layer. The vertical variation of TOC is positively correlated with the illite/montmorillonite mixed layer.

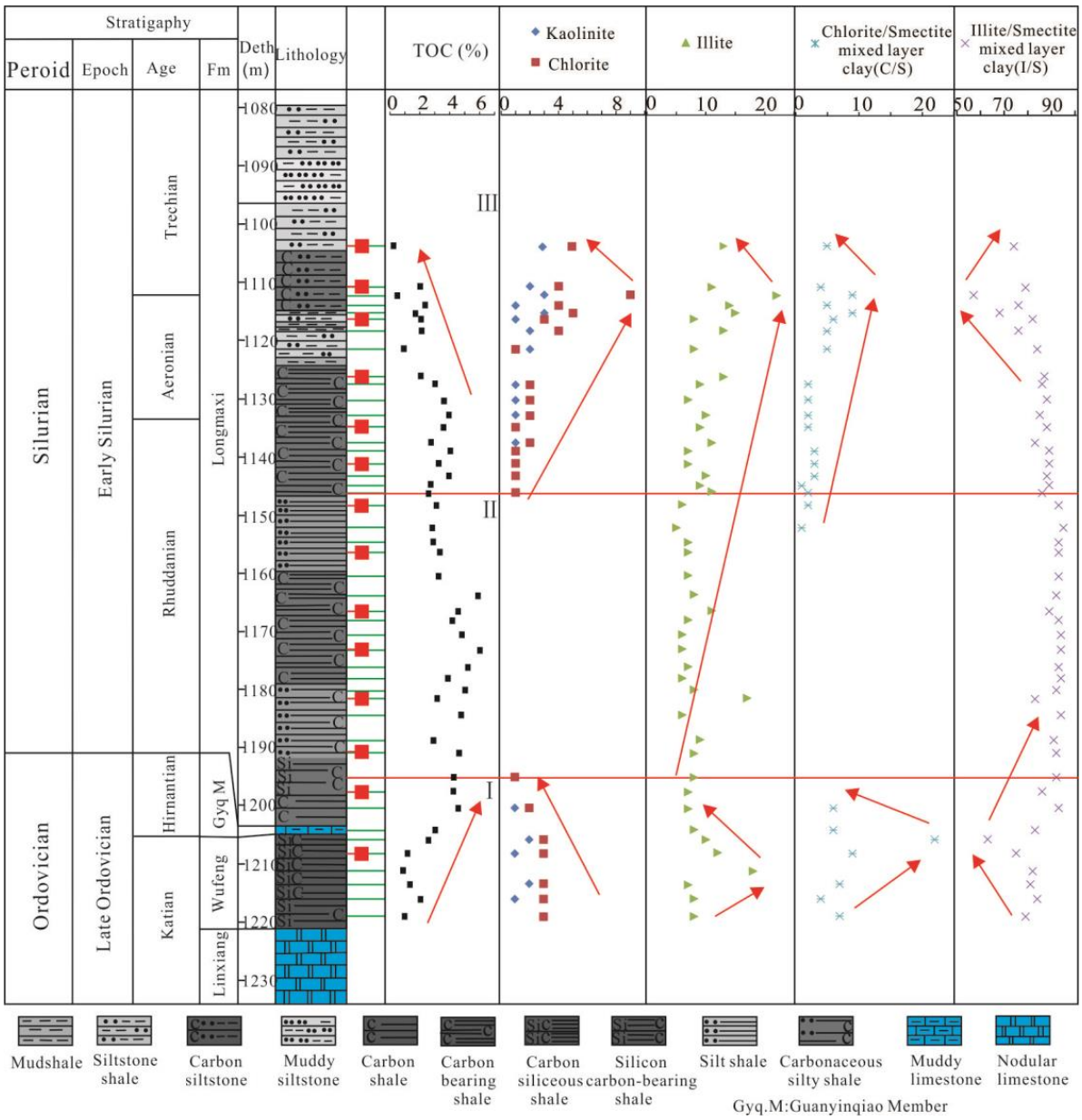

Figure 5. The vertical variation of black TOC and shale clay minerals in the Wufeng Formation–Longmaxi Formation.

4.4. Clay Mineral Indices Characteristics

When using clay minerals for paleoclimate reconstruction, it is important to ensure that the selected samples have not undergone significant diagenesis and to evaluate variations in provenance. Only when the samples have a low degree of diagenesis and the provenance location has not undergone significant changes can clay minerals be considered to reflect the paleoclimatic evolution in the study area [58,59]. Illite crystallinity (IC) is widely used as an indicator of metamorphic degree, with a threshold of 0.42° and 0.25° for the Kübler index of illite crystallinity. The metamorphic degree is divided into three regions: unmetamorphosed (>0.42°), incipient metamorphism (0.25°–0.42°), and shallow metamorphism (<0.25°). Only when clay minerals have not undergone significant metamorphic alteration can they be used to indicate paleoclimatic changes [58,59]. In this study, the crystallinity of illite was

measured using Jade software by calculating the full width at half maximum (FWHM) of the illite d (001) peak. The results show that the illite crystallinity of the Wufeng Formation–Longmaxi Formation in the study section was greater than 0.42°, indicating an unmetamorphosed zone. Therefore, it is considered that clay minerals in the study area are not affected by diagenesis. Additionally, major elements, as well as their ratios, are commonly used to study the provenance characteristics of sedimentary materials. The migration rates of elements in sediments vary significantly in different depositional environments. Al_2O_3 and TiO_2 are stable in water and can represent the input of terrigenous materials. Ratios of these elements with other elements can indicate whether there have been changes in the provenance area [60–62]. The fluctuation range and amplitude of the Al_2O_3/TiO_2 ratio in the study samples were small (Table 3 and Figure 6), indicating that there have been no significant changes in the provenance location in this area. Therefore, it is concluded that the clay minerals in the study area have a low degree of diagenetic alteration and the provenance has not undergone significant changes, making it effective in recording the paleoclimatic evolution in the Sichuan Basin during the Late Ordovician to Early Silurian period.

Table 3. Characteristics of clay minerals and oxide weathering indices.

Fm	Sample	TOC	[(S + I/S)/(I + C)]	I/C	CIA-error	CIA	CIW	PIA	LST (°C)	MAP/mm/yr	Al_2O_3/TiO_2
Longmaxi	YC1-1	0.24	0.72	2.60	68.94	67.69	90.23	85.36	12.21	227.40	14.44
	YC1-5	2.03	0.73	2.75	77.83	76.98	93.28	91.47	17.41	224.31	18.31
	YC1-7	0.50	0.71	2.44	/	/	□/	□/	□/	□/	□/
	YC1-9	2.37	0.78	3.50	/	/	□/	□/	□/	□/	□/
	YC1-12	1.72	0.75	3.00	/	/	□/	□/	□/	□/	□/
	YC1-14	2.10	0.73	2.67	41.67	39.06	58.89	16.49	−3.83	225.50	5.88
	YC1-17	2.14	0.76	3.25	/	/	□/	□/	□/	□/	□/
	YC1-19	0.95	0.89	8.00	/	/	□/	□/	□/	□/	□/
	YC1-24	2.09	0.93	13.00	45.04	41.32	75.00	−35.22	−2.56	225.36	5.18
	YC1-26	3.05	0.82	4.50	/	/	□/	□/	□/	□/	□/
	YC1-29	3.65	0.78	3.50	/	/	□/	□/	□/	□/	□/
	YC1-32	3.98	0.83	5.00	/	/	□/	□/	□/	□/	□/
	YC1-35	3.62	0.90	9.00	44.28	41.42	73.29	−15.79	−2.50	226.51	5.46
	YC1-39	2.79	0.85	5.50	/	/	□/	□/	□/	□/	□/
	YC1-41	4.09	0.88	7.00	/	/	□/	□/	□/	□/	□/
	YC1-44	3.31	0.88	7.00	69.60	68.73	85.46	80.79	12.79	224.75	18.92
	YC1-47	4.00	0.91	10.00	/	/	□/	□/	□/	□/	□/
	YC1-49	2.78	0.90	9.00	/	/	□/	□/	□/	□/	□/
	YC1-52	2.64	0.92	11.00	/	/	□/	□/	□/	□/	□/
	YC1-54	3.17	0.86	6.00	52.87	43.47	65.43	30.15	−1.36	226.90	7.07
	YC1-58	2.90	0.83	5.00	/	/	□/	□/	□/	□/	□/
	YC1-61	2.96	0.88	7.00	/	/	□/	□/	□/	□/	□/
	YC1-63	3.41	0.88	7.00	78.59	77.77	89.02	87.16	17.85	226.87	31.22
	YC1-68	3.33	0.88	7.00	/	/	□/	□/	□/	□/	□/
	YC1-72	5.97	0.89	8.00	/	/	□/	□/	□/	□/	□/
	YC1-74	4.64	0.92	11.00	75.42	74.41	88.81	86.13	15.97	225.71	24.16
	YC1-78	4.26	0.88	7.00	/	/	□/	□/	□/	□/	□/
	YC1-81	4.90	0.86	6.00	/	/	□/	□/	□/	□/	□/
	YC1-84	6.11	0.86	6.00	71.18	61.62	77.36	69.59	8.81	226.38	15.81
	YC1-86	5.31	0.88	7.00	/	/	□/	□/	□/	□/	□/
	YC1-89	3.97	0.86	6.00	/	/	□/	□/	□/	□/	□/
	YC1-92	5.13	0.89	8.00	/	/	□/	□/	□/	□/	□/
	YC1-94	3.26	0.94	17.00	73.46	72.67	84.30	81.31	15.00	227.01	26.32
	YC1-96	4.87	0.86	6.00	/	/	□/	□/	□/	□/	□/
	YC1-102	3.02	0.90	9.00	/	/	□/	□/	□/	□/	□/

Table 3. *Cont.*

Fm	Sample	TOC	[(S + I/S)/ (I + C)]	I/C	CIA-error	CIA	CIW	PIA	LST (°C)	MAP/ mm/yr	Al_2O_3/TiO_2
Wufeng	YC1-104	4.74	0.89	8.00	79.56	78.91	90.03	88.40	18.49	226.87	33.70
	YC1-109	4.38	0.89	8.00	/	/	□/	□/	□/	□/	□/
	YC1-114	4.36	0.88	7.00	80.49	79.60	88.78	87.32	18.87	227.82	39.58
	YC1-118	4.69	0.88	7.00	/	/	□/	□/	□/	□/	□/
	YC1-121	3.15	0.80	4.00	/	/	□/	□/	□/	□/	□/
	YC1-123	2.70	0.77	3.33	/	/	□/	□/	□/	□/	□/
	YC1-126	1.30	0.80	4.00	93.07	92.95	96.59	96.45	26.35	222.12	101.93
	YC1-128	1.01	0.95	18.00	/	/	□/	□/	□/	□/	□/
	YC1-132	1.47	0.70	2.33	/	/	□/	□/	□/	□/	□/
	YC1-134	2.18	0.73	2.67	/	/	□/	□/	□/	□/	□/
	YC1-136	1.12	0.73	2.67	/	/	□/	□/	□/	□/	□/

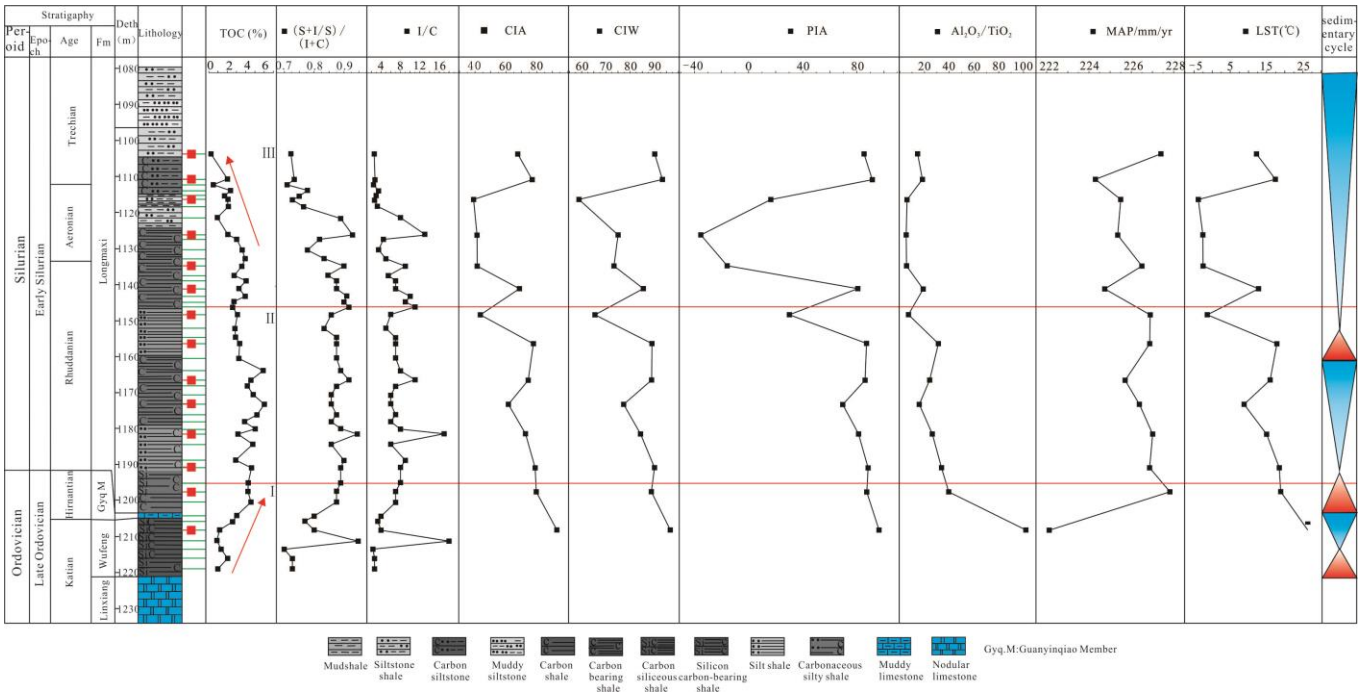

Figure 6. The relationship between weathering degree in Yucan-1 Well, land surface temperature (LST), and surface precipitation.

By calibrating and combining the chemical weathering indices of major elements and the climate indices derived from clay mineral composition ratios, it is possible to effectively reflect the relationship between weathering degree and paleoclimate in the study area. This approach can reveal the patterns of paleoclimatic changes in the Late Ordovician to Early Silurian period in the Sichuan Basin (Table 3).

5. Discussion

5.1. Clay Mineral Content and Paleoclimate

Clay minerals are usually produced by weathering in the weathering crust and can be used to indicate the degree of weathering and paleoclimate characteristics. Different mineral combinations and changes in content are sedimentary responses to the evolution of paleoclimate. Kaolinite is formed by the intense leaching of feldspar, pyroxene, and mica [63], and is formed under warm and humid high weathering conditions. Chlorite is unstable under oxidizing conditions [64] and can only be preserved in environments where chemical weathering is inhibited [63]. It is generally believed that an increase in the

relative content of chlorite and illite indicates a gradual drying of the climate [58]. Illite is formed under cold and dry climatic conditions [58,65]. If the climate further becomes warm and humid, illite will be transformed into kaolinite [66–68]. The Late Ordovician–Early Silurian period in the Sichuan Basin experienced the first mass extinction event since the Phanerozoic, with complex climate and environmental evolution. The shale of the Wufeng Formation–Longmaxi Formation in the study section in the study area records the relationship between complex climatic, environmental, and geological events during this period. Therefore, through the characteristics of oxides and clay minerals in the shale of the Wufeng Formation–Longmaxi Formation in the study section, the relationship between climate evolution and geological events during this period is revealed. Through the study of the clay mineral types and content characteristics of the Wufeng and Longmaxi Formations in the study section, it was found that montmorillonite, chlorite, illite, and Illite/montmorillonite mixed layer minerals were dominant (interval I), with relatively stable changes in relative trends. Some samples did not have kaolinite and chlorite minerals (Figure 5). There were low contents of illite at the bottom of the Wufeng Formation, which increased significantly at the boundary between the Wufeng Formation and the Longmaxi Formation and then decreased again. Organic carbon (TOC) contents changed from being poor in the Wufeng Formation to being enriched at the bottom of the Longmaxi Formation, indicating that warm–humid and cold–dry climates alternated during the early Wufeng Formation–Longmaxi Formation period. Chemical weathering and rainfall also alternated or coexisted, consistent with the rainfall index (MAP) shown in Figure 5, which was conducive to organic carbon enrichment. In the middle of the Longmaxi Formation (interval II), illite and illite/montmorillonite mixed layers were dominant, while kaolinite, chlorite, and chlorite/montmorillonite mixed layer minerals were absent (Figure 5). The absence of kaolinite indicates a decrease in rainfall and a colder climate. Terrestrial feldspar, pyroxene, and mica-lacked rainwater and did not undergo leaching; thus, they could not be transformed into kaolinite, consistent with the land surface rainfall index (MAP). The absence of chlorite and chlorite/montmorillonite mixed layers indicates that chemical weathering was inhibited, which was not conducive to the preservation of chlorite and also indicates a low degree of weathering and a cold and dry climate. Organic carbon (TOC) remained at an enriched level. This indicates a cold and dry climatic environment with a low chemical weathering capacity of terrestrial sources and relatively stable and low rainfall (Figure 6), which is conducive to organic carbon enrichment. In the upper part of the Longmaxi Formation (interval III), kaolinite, chlorite, illite, chlorite/montmorillonite mixed layer, and illite/montmorillonite mixed layer minerals were dominant (Figure 5), all showing an increasing–decreasing trend upwards. The rainfall index (MAP) also showed an increasing–decreasing trend (Figure 6). Organic carbon (TOC) contents changed from being enriched to being low, indicating that the climate in the upper part of the Longmaxi Formation changed from warm–humid–rainy to cold–dry–rainy to warm–humid–rainy. The chemical weathering degree of terrestrial material became stronger and stronger, which was not conducive to organic carbon (TOC) enrichment.

5.2. Clay Mineral Specific Values and Paleoclimate

In addition to the types of clay minerals that can be used to indicate different climatic environments, some ratios of clay mineral content can also be used as weathering indices to measure the degree of chemical weathering (montmorillonite/illite ratio, clay mineral/quartz ratio, illite chemical index). Higher values of these indices indicate stronger chemical weathering [66]. In addition, diagenesis is also an important factor affecting the composition of clay minerals. The value of illite crystallinity can be used to measure its degree of alteration and effectiveness [65]. As discussed in Section 4.1, the crystallinity of illite is greater than 0.42 degrees, indicating that the parameter indicators of clay minerals are reliable and effective. In the early phases of soil formation by weathering, chlorite is easily weathered into vermiculite, montmorillonite, vermiculite/chlorite mixed layer minerals, and other clay minerals. Illite is easily preserved due to its high resistance to

weathering and the weathering rate of chlorite is greater than that of illite. Therefore, the illite/chlorite (I/C) and (montmorillonite + illite/montmorillonite mixed layer)/(illite + chlorite) (S + I/S)/(I + C) indices are used to determine the weathering intensity and soil-forming environment of clay minerals. The larger the I/C and (S + I/S)/(I + C), the warmer and more humid the climate; otherwise, the climate is cold and dry [58,69]. The overall trend of I/C and (S + I/S)/(I + C) in clay minerals in the study section is increasing–decreasing–stable–increasing–decreasing (Table 3). The I/C and (S + I/S)/(I + C) values of clay minerals in the bottom of the Wufeng Formation–Longmaxi Formation in the study section (interval I) are increasing–decreasing. Organic carbon (TOC) content changes from being low to being enriched, indicating a transition from a cold–dry to a warm–humid climatic environment from the bottom of the Wufeng Formation–Longmaxi Formation, followed by a return to a cold–dry climatic environment, which is conducive to organic carbon (TOC) enrichment. In the middle part of the Longmaxi Formation (interval II), the I/C and (S + I/S)/(I + C) values of clay minerals did not change much and were relatively stable (Figure 6). Organic carbon (TOC) remained at a stable enriched level, indicating that this section maintained the cold–dry climatic environment during sedimentation at the bottom of the Longmaxi Formation, which was conducive to organic carbon (TOC) enrichment. In the upper part of the Longmaxi Formation (interval III), the gradual decrease in both the (I/C) and (S + I/S)/(I + C) values of clay minerals indicates a shift towards a colder and drier climate. This shift was accompanied by a transition from organic carbon (TOC) enrichment to depletion, suggesting an unfavorable environment for TOC accumulation. The overall climatic pattern of the Wufeng Formation–Longmaxi Formation follows a sequence of cold and dry, warm and humid, and then returning to cold and dry conditions. The transition from cold and dry to warm and humid in the Wufeng Formation aligns with a subsequent sudden cooling event, which correlates with the global glaciation during the Huronian Period. While the lower part of the Longmaxi Formation still maintained the cold climate environment from the Huronian Period, the upper part experienced a shallower sea and a shift towards a warmer and more humid climate. However, at the top of the Longmaxi Formation, the climate became relatively colder and drier. This climatic shift is supported by the lowest values of (I/C) and (S + I/S)/(I + C) for clay minerals, which are consistent with the climatic indications based on clay mineral content. Moreover, this indicates a significant accumulation of organic carbon (TOC) following the Huronian glaciation that occurred after the Wufeng Formation. As the upper part of the Longmaxi Formation transitioned from cold and dry to warm and humid conditions, weathering intensified, and sea levels decreased. These factors hindered the enrichment of organic carbon (TOC), impeding its accumulation.

5.3. Chemical Weathering Index and Paleoclimate

The values of CIA (chemical index of alteration), CIW (chemical index of weathering), and PIA (plagioclase index of alteration) typically range from 50 to 100. A CIA value of 50 indicates minimal chemical weathering, while higher CIA values indicate a greater degree of loss of mobile elements through leaching [44,70]. The migration of elements is closely related to climate, and different climatic environments result in distinct CIA values. Generally, higher CIA values indicate a warmer and more humid climate, while lower values correspond to colder and drier conditions. The presence of potassium elements leads to an increase in CIA values, and, to provide a comprehensive assessment, Nesbitt [61] proposed the use of the CIW index, which reflects the paleoclimate of the source area and has a tendency towards warm and humid conditions. However, Fedo et al. [57] suggested that CIW, which excludes K_2O, does not account for the influence of the Al element in potassic feldspar. For samples rich in potassic feldspar in the source rocks, regardless of weathering processes, the CIW values would be high. In such cases, a separate weathering index, PIA (plagioclase index of alteration), is needed to assess the weathering of easily weathered plagioclase. Generally, higher PIA values indicate a warm and humid climate, while lower values suggest cold and arid conditions. Studies have shown that CIA values

can effectively reflect the climate evolution between glacial and interglacial periods [69], and the Late Ordovician to Early Silurian period experienced a global Hirnantian glaciation event [31]. Therefore, in this study, CIA, CIA-error, CIW, and PIA indices were employed to investigate the paleoclimate evolution during the Late Ordovician to Early Silurian period and reveal the climatic controlling factors of the first mass extinction event.

At the bottom of the Yucan-1 Well, in the Wufeng Formation–Longmaxi Formation (interval I), the values of chemical weathering indices (CIA, CIA-error, CIW, and PIA) are high (Figure 6), indicating a warm climate with increased mean annual precipitation (MAP) and land surface temperature (LST). After the Hirnantian glaciation, the values of CIA, CIA-error, CIW, and PIA rapidly decreased, along with a decrease in LST and an increase in MAP, indicating a shift to a cold and arid climate. This suggests that the climate did not return to its previous warm and humid state after the Hirnantian glaciation, which may have been a controlling factor in the first mass extinction event at the end of the Late Ordovician to Early Silurian. Additionally, this climate shift favored the enrichment of organic carbon (TOC), transitioning from depletion to accumulation. In the middle section (interval II) of the Longmaxi Formation, compared to the previous period, the values of CIA, CIA-error, CIW, PIA, MAP, and LST are relatively higher (Figure 6), indicating a shift towards a warm and humid climate. Subsequently, these values gradually decrease, indicating a transition to a cold, arid, and less rainy climate. The TOC content remains consistently enriched, suggesting that the middle section of the Longmaxi Formation (interval II) was mainly characterized by a cold and arid climate with reduced weathering. Rainfall and surface temperature remained relatively stable, favoring the accumulation of organic carbon (TOC). In the upper section (interval III) of the Longmaxi Formation in the study section, the curves of CIA, CIA-error, CIW, PIA, MAP, and LST show a fluctuating trend of increase and decrease (Figure 6). Compared to the bottom (interval I) and middle (interval II) sections of the Wufeng and Longmaxi Formations, the weathering indices CIA, CIA-error, CIW, PIA, MAP, and LST decrease, indicating a significant reduction in chemical weathering and a colder and drier climate (Figure 6). Towards the uppermost part of the Longmaxi Formation, the climate changed to a warm and humid environment, accompanied by noticeable increases in rainfall and surface temperatures and enhanced surface weathering. The organic carbon content (TOC) shifts from enrichment to depletion. This indicates that the climate in the upper section of the Longmaxi Formation was cold and arid, gradually recovering to the warm and humid environment of the Wufeng Formation period at the top, which was unfavorable for the enrichment of organic carbon (TOC).

In summary, the characteristics of clay mineral content, clay mineral ratios, chemical weathering indices, surface temperature, and atmospheric precipitation in the shale of the Wufeng Formation–Longmaxi Formation in the Yucan-1 Well show that the climate transitioned from warm and humid to cold and dry from the Wufeng Formation to the bottom of the Longmaxi Formation (interval I). The climate in the middle part of the Longmaxi Formation (interval II) was relatively stable, dominated by cold and dry conditions, with relatively lower rainfall and surface temperatures. The climate in the upper part of the Longmaxi Formation (interval III) became colder and drier. Surface temperature first decreased and then increased. Surface rainfall first decreased and then increased. The climate at the top became warmer and returned to the climatic environment of the Wufeng Formation period. The transformation of organic carbon (TOC) from depletion to enrichment and then back to depletion from the Wufeng Formation–Longmaxi Formation also indicates that a warm and humid environment is not conducive to the enrichment of organic carbon (TOC), while a cold and dry climate is conducive to the enrichment of organic carbon (TOC). Climate cooling is also proven to be the main cause of the Late Ordovician (Hernantian) mass extinction.

5.4. Late Ordovician–Early Silurian Climate Cools

The Late Ordovician–Early Silurian transition period was an important geological historical period, during which the first and only mass extinction event involving glaciers

occurred in the Phanerozoic [12], accompanied by geological events such as oceanic anoxia, sea level rise and fall, and glaciation [12,31,40]. Positive isotope shifts occurred in carbonate rock carbon isotopes and sulfate rock sulfur isotopes in the late Katian phase [71], negative shifts occurred in sedimentary uranium isotopes [12,72], and paleomagnetic data from the South China Plate and other global plates [72] indicate that the mass extinction event was related to changes in the marine ecosystem and terrestrial climate. The chemical weathering indices CIA-error, (S + I/S)/(I + C), MAP, and LST of the Wufeng Formation–Longmaxi Formation shale in the study section in South China indicate that the overall transition from the Wufeng Formation to the Longmaxi Formation was from warm and humid to cold and dry, with a significant decrease in temperature and rainfall and a transition from deep sea shelf to shallow sea shelf. The first section (interval I) shows that the climate of the Wufeng Formation was relatively warm and humid, transitioning from high to low temperatures. Surface weathering was strong, rainfall was low, organic carbon was low, and seawater oxidation was strong, consistent with global sedimentary U and S isotope changes during this period. Sea levels decreased to their lowest point in the late Wufeng Formation, with the appearance of terrestrial glaciers [12,73]. This indicates that the climate of the Wufeng period in South China turned cold and dry, with a decrease in surface temperature. Qiu et al. [74] believed that this period transformed from oxygen-rich to oxygen-deficient, leading to a large extinction of marine organisms that were not adapted to cold environments. Kozik et al. [12] believed that this extinction event experienced two phases of pulse extinction: LOME-1 and LOME-2, both related to climate cooling and consistent with the results of this study. The second section (interval II) shows that the CIA-error, (S + I/S)/(I + C), MAP, and LST indicators of the Longmaxi Formation were relatively stable compared to the first section (interval I), showing an overall process of gradual change. Among them, CIA-error and LST showed a significant positive correlation. As chemical weathering decreased, the climate became colder and drier and temperature decreased. Organic carbon (TOC) showed a significant positive correlation with (S + I/S)/(I + C) and MAP. Rainfall increased and sea levels recovered from low to high, consistent with global changes during this period (Figure 7A–G). This indicates that the early Longmaxi Formation continued the cold and dry climate of the Hirnantian Ice Age. The enrichment of organic matter during this period was due to multiple volcanic activities [75]. Volcanic ash containing large amounts of sulfides drifted into the atmosphere and fell into the ocean with rainwater, causing oceanic anoxia (sulfidation) and preserving a large amount of organic matter. The third interval (interval III) shows that compared to the second interval, there were significant changes in CIA-error, (S + I/S)/(I + C), MAP, and LST indicators in the upper part of the Longmaxi Formation. Overall, organic carbon (TOC) showed a positive correlation with (S + I/S)/(I + C) and MAP. It experienced a rising–falling–rising trend. Weathering degree (CIA-error) and LST were correlated. There was a strengthening–weakening–strengthening process and sea levels decreased. This indicates that in the upper part of the Longmaxi Formation (interval III), the climate changed from warm–humid to cold–dry, and rainfall decreased. The input of volcanic ash carried by rainfall into the ocean decreased. Seawater became shallower. The amount of oxygen dissolved in seawater increased due to increases in atmospheric oxygen, leading to the transformation of the oceanic environment from anoxic (sulfidation) to oxygenated (oxidation) [1,40]. Organic matter decomposed and organic matter content decreased.

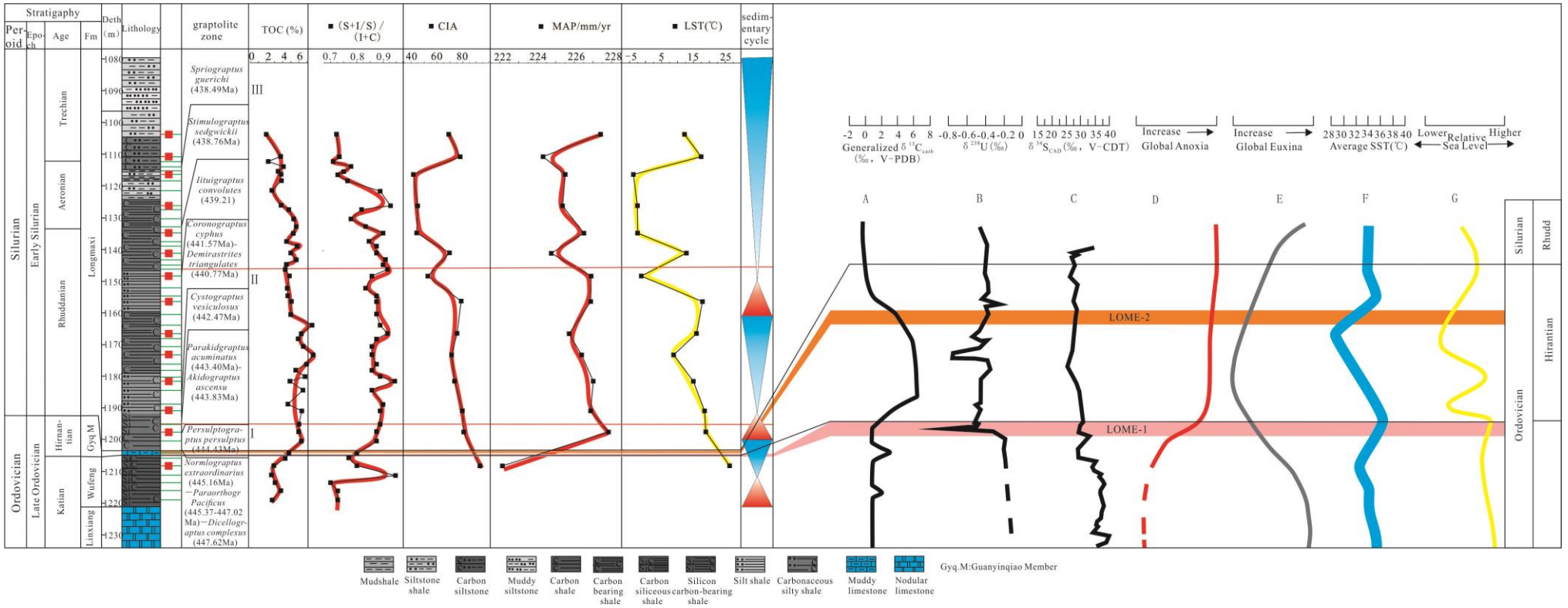

Figure 7. The relationship between the degree of land surface weathering during the late Ordovician Silurian period and sea levels, land surface temperatures, land surface rainfall, biological extinction, and climate. (**A**) The $\delta^{13}C$ data are replotted from Kozik et al. [12]. (**B**) The $\delta^{238}U$ data are replotted from Bartlett et al. [72] (purple dots) and Lu et al. [76] (purple triangles). (**C**) The $\delta^{34}S_{CAS}$ datasets from this study are the green dots/lines representing the Kärdla drill core and the orange dots/lines representing the Monitor Range section. The blue dots/lines are from the western Anticosti Island section (replotted from Jones and Fike [71]); brown inverted triangles are brachiopod-CAS; brown squares are bulk-CAS data from Kampschulte and Strauss [77]; yellow stars are brachiopod-CAS; and yellow triangles are bulk-CAS from Present et al. [78]. Note the clear overlap in $\delta^{34}S_{CAS}$ values from bulk- and brachiopod-CAS datasets throughout the upper Katian-Hirnantian phases. (**D**) Generalized changes in the extent of global marine anoxia. (**E**) Generalized changes in the extent of global marine euxinia. (**F**) Average sea surface temperature data replotted from Finnegan et al. [5]. (**G**) Eustatic sea levels from Goldman et al. [79].

The characteristics of CIA-error, (S + I/S)/(I + C), MAP, and LST indicators in the shale of the Wufeng Formation–Longmaxi Formation in the study section show an overall decreasing trend, indicating that during the Wufeng Formation period, the climate changed from warm and humid to cold and dry. The cooling of marine biology led to the unavailability of marine organisms to adapt to the new environment. This was accompanied by volcanic eruptions that lead to oceanic anoxic and sulfuric events [75]. The cold and dry climate may have persisted until approximately 438.76 Ma (Stimulograptus sedgwickii Zone) (Figure 7), leading to the continuous extinction of organisms. This is consistent with Kozik et al.'s [12] results on weathering intensity and glaciation-induced climate cooling promoting mass extinction in multiple global basins. The study of the climate cooling event in South China further verifies that two climate cooling events led to mass extinctions. The subsequent continuous cooling may also have led to the extinction of some organisms, but not to extinction events as significant as the LOME extinction event.

6. Conclusions

(1) Based on logging curves and lithological characteristics, the Wufeng Formation–Longmaxi Formation in the Yucan-1 Well is divided into three third-order sequences: SQ1, SQ2, and SQ3. SQ1 is located in the Wufeng Formation and developed TST and RST, dominated by deep-water calcareous shelf microfacies and shallow-water calcareous shelf. SQ2 mainly developed TST and RST, dominated by deep-water calcareous shelf and deep-water sandy shelf microfacies. SQ3 mainly developed TST and RST, dominated by deep-water sandy shelf, deep-water calcareous shelf, shallow-water calcareous shelf, and shallow-water sandy shelf microfacies. In the Guanyinqiao member, the sea level was at its lowest point, and then recovered to the sea level height of the early Wufeng Formation, followed by a decrease in sea levels. This reflects the overall fluctuation in sea levels from high–low–high–low in the Wufeng Formation–Longmaxi Formation.

(2) Based on the characteristics of TOC, clay minerals and oxide content, (I/C), (S + I/S)/(I + C), CIA, CIA-error, CIW, PIA, MAP, and LST parameters in the shale of the Wufeng Formation–Longmaxi Formation, the Wufeng Formation–Longmaxi Formation is divided into three sedimentary periods. The first period is the Wufeng Formation. Weathering degree, surface temperatures, and rainfall gradually decreased. The climate changed from warm and humid to cold and dry. This corresponds to two pulse mass extinction events and was a stage of increasing organic carbon burial. The second period is the bottom of the Longmaxi Formation. Weathering degrees, surface temperatures, and rainfall were at low levels. Later, the period was dominated by a dry and cold climate. It was the main stage of organic carbon burial. The third period is from the upper part to the top of the Longmaxi Formation. Weathering degrees, surface temperatures, and rainfall gradually increased. The climate changed from cold and dry to warm and humid. Organic carbon burial gradually decreased and sea levels decreased.

(3) Based on the paleoclimate evolution characteristics of the shale of the Wufeng Formation–Longmaxi Formation, the study of the climate cooling event in the late Ordovician–Early Silurian period has deepened our understanding of the first pulse mass extinction event in the Phanerozoic. It is believed that after the pulse mass extinction at the end of the late Ordovician period (LOME-1, LOME-2), the cold and dry climate may have persisted until approximately 438.76 Ma (Stimulograptus sedgwickii Zone), causing a second extinction of organisms that escaped the late Ordovician extinction. The extent may not be as severe as the LOME extinction. Afterwards, the climate returned to the warm and humid climatic environment from before the LOME extinction.

Author Contributions: Conceptualization: Z.Z. and H.W.; methodology, Z.Z.; software, Y.G.; validation, D.Z. and J.Z.; formal analysis, Z.Z.; investigation, Z.Z.; resources, Z.Z. and Y.G.; data curation, Z.Z.; writing—original draft preparation, Z.Z.; writing—review and editing, Y.G. and Z.Z.; visualization, Z.Z. and C.Z.; supervision, Y.G.; project administration, Y.G.; funding acquisition, Z.Z. and D.Z. All authors have read and agreed to the published version of the manuscript.

Funding: This work was supported by the Graduate Innovation Program of China University of Mining and Technology (grant no. 2022WLKXJ002), the Postgraduate Research & Practice Innovation Program of Jiangsu Province (grant no. KYCX22_2600), the Jiangsu Natural Science Foundation project (grant no. SBK2021045820), and the Chongqing Natural Science Foundation General Project (grant no. cstc2021jcyj- msxm X0624).

Institutional Review Board Statement: Not applicable.

Informed Consent Statement: Not applicable.

Data Availability Statement: The data presented in this study are contained within this article.

Acknowledgments: We thank Xun-lian Wang for his encouragement and constructive comments on the manuscript. We would also like to thank the anonymous reviewers for their comments which helped to improve the manuscript.

Conflicts of Interest: The authors declare that they have no known competing financial interests or personal relationships that could have appeared to influence the work reported in this paper.

References

1. Rong, J.Y.; Fan, J.X.; Miller, A.I.; Li, G.X. Dynamic patterns of latest Proterozoic-Paleozoic-Early Mesozoic marine biodiversity in South China. *Geol. J.* **2007**, *42*, 431–454.
2. Berner, R.A. Atmospheric carbon dioxide levels over phanerozoic time. *Science* **1990**, *249*, 1382–1386. [CrossRef]
3. Yapp, C.J.; Poths, H. Ancient atmospheric CO_2 pressures inferred from natural goethites. *Nature* **1992**, *355*, 342–344. [CrossRef]
4. Brenchley, P.J.; Marshall, J.D.; Carden, G.A.F.; Robertson, D.B.R.; Long, D.G.F.; Meidla, T.; Hints, L.; Anderson, T.F. Bathymetric and isotopic evidence for a short-lived Late Ordovician Glaciation in a Greenhouse Period. *Geology* **1994**, *22*, 295–298. [CrossRef]
5. Finnegan, S.; Bergmann, K.; Eiler, J.M.; Jones, D.S.; Fike, D.A.; Eisenman, I.; Hughes, N.C.; Tripati, A.K.; Fischer, W.W. The magnitude and duration of Late Ordovician-Early Silurian glaciation. *Science* **2011**, *331*, 903–906. [CrossRef]
6. Stanley, S.M. Temperature and biotic crises in the marine realm. *Geology* **1984**, *12*, 205–208. [CrossRef]
7. Wilde, P.; Berry, W.B.N. Destabilization of the oceanic density structure and its significance to marine "extinction" events. Palaeogeogr. *Palaeoclimatol. Palaeoecol.* **1984**, *48*, 143–162. [CrossRef]
8. Sheehan, P.M. The Late Ordovician mass extinction. *Annu. Rev. Earth Planet Sci.* **2001**, *29*, 331–364. [CrossRef]
9. Histon, K.; Klein, P.; Schönlaub, H.P.; Huff, W.D. Lower Palaeozoic K-bentonites from the Carnic Alps, Austria. *Aust. J. Earth Sci.* **2007**, *100*, 26–42.
10. Huff, W.D. Ordovician K-bentonites: Issues in interpreting and correlating ancient tephras. *Quat. Int.* **2008**, *178*, 276–287. [CrossRef]
11. Hu, Y.H.; Sun, W.D.; Ding, X.; Wang, F.Y.; Ling, M.X.; Liu, J. Volcanic event at the OrdovicianSilurian boundary: The message from K-bentonite of Yangtze Block. *Acta Pet. Sin.* **2009**, *25*, 3298–3308, (In Chinese with English abstract).
12. Kozik, N.P.; Gill, B.C.; Owens, J.D.; Lyons, T.W.; Young, S.A. Geochemical records reveal protracted and differential marine redox change associated with Late Ordovician climate and mass extinctions. *AGU Adv.* **2022**, *3*, e2021AV000563. [CrossRef]
13. Bond, D.P.G.; Grasby, S.E. Late Ordovician mass extinction caused by volcanism, warming, and anoxia, not cooling and glaciation. *Geology* **2020**, *48*, 777–781. [CrossRef]
14. Longman, J.; Mills, B.J.W.; Manners, H.R.; Gernon, T.M.; Palmer, M.R. Late Ordovician climate change and extinctions driven by elevated volcanic nutrient supply. *Nat. Geosci.* **2021**, *14*, 924–929. [CrossRef]
15. Saupe, E.E.; Qiao, H.J.; Donnadieu, Y.; Farnsworth, A.; Kennedy-Asser, A.; Ladant, J.B.; Lunt, D.J.; Pohl, A.; Valdes, P.; Finnegan, S. Extinction intensity during Ordovician and Cenozoic glaciations explained by cooling and palaeogeography. *Nat. Geosci.* **2020**, *13*, 65–70. [CrossRef]
16. Lenton, T.M.; Crouch, M.; Johnson, M.; Pires, N.; Dolan, L. First plants cooled the Ordovician. *Nat. Geosci.* **2012**, *5*, 86–89. [CrossRef]
17. Shen, J.; Pearson, A.; Henkes, G.A.; Zhang, Y.G.; Chen, K.; Li, D.; Wankel, S.D.; Finney, S.C.; Shen, Y. Improved efficiency of the biological pump as a trigger for the Late Ordovician glaciation. *Nat. Geosci.* **2018**, *11*, 510–514. [CrossRef]
18. Harperb, D.A.T.; Hammarlund, E.U.; Rasmussen, C.M.Ø. End Ordovician extinctions: A coincidence of causes. *Gondwana Res.* **2014**, *25*, 1294–1307. [CrossRef]
19. He, L.; Wang, Y.P.; Chen, D.F. Geochemical features of sedimentary environment and paleoclimate during Late Ordovician to Early Silurian in southern Sichuan Basin. *Geochimica* **2021**, *50*, 623–634. (In Chinese)

20. Yang, X.R.; Yan, D.T.; Zhang, L.W.; Zhang, B.; Xu, H.W.; Liu, W.H.; Yun, J.L. The Genesis of Hirnantian Glaciation and Paleo-Ocean Environment During Ordovician-Silurian Transition. *Acta Sedimentol. Sin.* **2018**, *36*, 319–332. (In Chinese)
21. Pohl, A.; Nardin, E.; Vandenbroucke, T.R.A.; Donnadieu, Y. High dependence of Ordovician ocean surface circulation on atmospheric CO_2 levels. *Palaeogeogr. Palaeoclimatol. Palaeoecol.* **2016**, *58*, 39–51. [CrossRef]
22. Tobin, K.J.; Bergstr, M.S.M. Implications of Ordovician (≈460 Myr) marine cement for constraining seawater temperature and atmospheric pCO_2. *Palaeogeogr. Palaeoclimatol. Palaeoecol.* **2002**, *181*, 399–417. [CrossRef]
23. Tobin, K.J.; Bergstr, M.S.M.; De, L.; Garza, P.A. Mid-Caradocian (453 Ma) drawdown in atmospheric pCO_2 without ice sheet development? *Palaeogeogr. Palaeoclimatol. Palaeoecol.* **2005**, *226*, 187–204. [CrossRef]
24. Yapp, C.J.; Poths, H. Carbon isotopes in continental weathering environments and variations in ancient atmospheric CO_2 pressure. *Earth Planet. Sci. Lett.* **1996**, *137*, 72–82. [CrossRef]
25. Gibbs, M.T.; Barron, E.J.; Kump, L.R. An atmospheric pCO2 threshold for glaciation in the Late Ordovician. *Geology* **1997**, *25*, 447–450. [CrossRef]
26. Herrmann, A.D.; Patzkowsky, M.E.; Pollard, D. Obliquity forcing with 8-12 times preindustrial levels of atmospheric pCO_2 during the Late Ordovician glaciation. *Geology* **2003**, *31*, 485–488. [CrossRef]
27. Torsvik, T.H.; Cocks, L.R. Gondwana from top to base in space and time. *Gondwana Res.* **2013**, *24*, 999–1030. [CrossRef]
28. Li, Y.F.; Schieber, J.; Fan, T.L.; Li, Z.Y.; Zhang, J.P. Regional depositional changes and their controls on carbon and sulfur cycling across the Ordovician-Silurian boundary, northwestern Guizhou, South China. *Palaeogeogr. Palaeoclimatol. Palaeoecol.* **2017**, *485*, 816–832. [CrossRef]
29. Rong, J.Y.; Chen, X.; Wang, Y.; Zhan, R.; Liu, J.; Huang, B.; Tang, P.; Wu, C.; Wang, G. Northward expansion of Central Guizhou Old land through the Ordovician and Silurian transition: Evidence and implications. *Sci. China Earth Sci.* **2011**, *41*, 1407–1415.
30. Yan, D.; Chen, D.; Wang, Q.; Wang, J. Large-scale climatic fluctuations in the latest Ordovician on the Yangtze block, south China. *Geology* **2010**, *38*, 599–602. [CrossRef]
31. Zou, C.N.; Dong, D.Z.; Wang, Y.M.; Li, X.J.; Huang, J.L.; Wang, S.H.; Guang, Q.Z.; Zhang, C.C.; Wang, H.Y.; Liu, H.L.; et al. Shale gas in China: Characteristics, challenges and prospects (I). *Pet. Explor. Dev.* **2015**, *42*, 753–767. [CrossRef]
32. Zhang, S.; Barnes, C.R. Late Ordovician-Early Silurian (Ashgillian-Llandovery) sea level curve derived from conodont community analysis, Anticosti Island, Québec. *Palaeogeogr. Palaeoclimatol. Palaeoecol.* **2002**, *180*, 5–32. [CrossRef]
33. Deng, Y.Y.; Fan, J.X.; Zhang, S.H.; Fang, X.; Chen, Z.Y.; Shi, Y.K.; Wang, H.W.; Wang, X.B.; Yang, J.; Hou, X.D.; et al. Timing and patterns of the great Ordovician biodiversification event and Late Ordovician mass extinction: Perspectives from South China. *Earth Sci. Rev.* **2021**, *220*, 103743. [CrossRef]
34. Rong, J.Y. Ecostratigraphic evidence of regression and influence of glaciation of Late Ordovician in the Upper Yangtze area. *Stratigr. J.* **1984**, *8*, 9–20.
35. Rasmussen, C.M.Ø.; Kröger, B.; Nielsen, M.L.; Colmenar, J. Cascading trend of Early Paleozoic marine radiations paused by Late Ordovician extinctions. *Proc. Natl. Acad. Sci. USA* **2019**, *116*, 7207–7213. [CrossRef]
36. Vandenbroucke, T.R.A.; Armstrong, H.A.; Williams, M.; Paris, F.; Zalasiewicz, J.A.; Sabbe, K.; Nolvak, J.; Challands, T.J.; Verniers, J.; Servais, T. Polar foront shift and atmospheric CO_2 during the glacial maximum of the Early Paleozoic Icehouse. *Proc. Natl. Acad. Sci. USA* **2010**, *107*, 14983–14986. [CrossRef]
37. Stanley SM Climatic cooling and mass extinction of Paleozoic reef communities. *Palaios* **1988**, *3*, 228–232. [CrossRef]
38. Kump, L.R.; Arthur, M.A.; Patzkowsky, M.E.; Gibbs, M.T.; Pinkus, D.S.; Sheehan, P.M. A weathering hypothesis for glaciation at high atmospheric pCO_2 during the Late Ordovician. *Palaeogeogr. Palaeoclimatol. Palaeoecol.* **1999**, *152*, 173–187. [CrossRef]
39. Brenchley, P.J. High-resolution stable isotope stratigraphy of Upper Ordovician sequences: Constraints on the timing of bioevents and environmental changes associated with mass extinction and glaciation. *Geol. Soc. Am. Bull.* **2003**, *115*, 89–104. [CrossRef]
40. Zou, C.N.; Qiu, Z.; Poulton, S.W.; Dong, D.Z.; Wang, H.Y.; Chen, D.Z.; Lu, B.; Shi, Z.S.; Tao, H.F. Ocean euxinia and climate change "double whammy" drove the Late Ordovician mass extinction. *Geology* **2018**, *46*, 535–538. [CrossRef]
41. Luo, G.M.; Algeo, T.J.; Zhan, R.B.; Yan, D.T.; Huang, J.H.; Liu, J.S.; Xie, S.C. Perturbation of the marine nitrogen cycle during the Late Ordovician glaciation and mass extinction. *Palaeogeogr. Palaeoclimatol. Palaeoecol.* **2016**, *448*, 339–348. [CrossRef]
42. Xiong, X.H.; Wang, J.; Xiong, G.Q.; Wang, Z.J.; Men, Y.P.; Zhou, X.L.; Zhou, Y.X.; Yang, X.; Deng, Q. Geological characteristics and exploration direction of shale gas in Wufeng Formation-Longmaxi Formation in northeast Chongqing. *Acta Geol. Sin.* **2018**, *92*, 1948–1958. (In Chinese)
43. Li, G. Simulation Study on Shale Reservoir Characteristics and Pore Evolution of Longmaxi Formation in Chengkou Area, Northeast Chongqing. Master's Thesis, China University of Mining and Technology, Xuzhou, China, 2019. (In Chinese).
44. Grim, R.E. *Crystal Structures of Clay Minerals and Their X-ray Identification*; Brindley, G.W., Brown, G., Eds.; Mineralogical Society: London, UK, 1980; 495p.
45. Johns, W.D.; Grim, R.E.; Bradley, W.F. Quantitative estimations of clay minerals by diffraction methods. *J. Sediment. Res.* **1954**, *24*, 242–251.
46. Biscaye, P.E. Mineralogy and sedimentation of recent deep-sea clay in the Atlantic Ocean and Adjacent Seas and Oceans. *Geol. Soc. Am. Bull.* **1965**, *76*, 803–832. [CrossRef]
47. Kübler, B.; Les, A. indicateurs de métamorphisme. *Rev. L'Inst. Fr. Pét.* **1964**, *19*, 1093–1112.
48. Wang, H.J.; Zhou, J. On the indices of illite crystallinity. *Acta Petrol. Sin.* **1998**, *14*, 395–405. (In Chinese)

49. Wang, P.; Du, Y.; Yu, W.; Algeo, T.J.; Zhou, Q.; Xu, Y.; Qi, L.; Yuan, L.; Pan, W. The chemical index of alteration (CIA) as a proxy for climate change during glacial-interglacial transitions in Earth history. *Earth Sci. Rev.* **2020**, *201*, 103032. [CrossRef]
50. Mclennan, S.M. Weathering and global denudation. *J. Geol.* **1993**, *101*, 295–303. [CrossRef]
51. Panahi, A.; Young, G.M.; Rainbird, R.H. Behavior of major and trace elements (including REE) during Paleoproterozoic pedogenesis and diagenetic alteration of an Archean granite near Ville Marie, Quebec, Canada. *Geochim. Cosmochim. Acta* **2000**, *64*, 2199–2220. [CrossRef]
52. Yang, J.H.; Peter, A.C.; Du, Y.H.; Feng, B.; Yan, J.X. Global continental weathering trends across the Early Permian glacial to post glacial transition: Correlatinghigh-and low-paleolatitude sedimentary record. *Geology* **2014**, *42*, 835–838. [CrossRef]
53. Harnois, L. The CIW index: A new chemical index of weathering. *Sediment. Geol.* **1988**, *55*, 319–322. [CrossRef]
54. Sheldon, N.D.; Retallack, G.; Tanaka, S. Geochemical climofunctions from North American soils and application to paleosols across the Eocene-Oligocene boundary in Oregon. *J. Geol.* **2002**, *110*, 687–696. [CrossRef]
55. Garzanti, E.; Padoan, M.; Setti, M.; Najman, Y.; Peruta, L.; Villa, I.M. Weathering geochemistry and Sr-Nd fingerprints of equatorial upper Nile and Congo muds. *Geochem. Geophys. Geosyst.* **2013**, *14*, 292–316. [CrossRef]
56. Fagel, N. Chapter Four Clay Minerals, Deep Circulation and Climate. In *Developments in Marine Geology*; Elsevier: Amsterdam, The Netherlands, 2007; pp. 139–176.
57. Fedo, C.M.; Nesbitt, H.W.; Young, G.M. Unraveling the effects of potassium metasomatism in sedimentary rocks and paleosols, with implications for paleoweathering conditions and provenance. *Geology* **1995**, *23*, 921–924. [CrossRef]
58. Chen, T.; Wang, H.; Zhang, Z.Q. Clay minerals as indicators of paleoclimate. *Acta Petrol. Mineral.* **2003**, *22*, 416–420. (In Chinese)
59. Liu, L.H. Crystallinity of Illite and Clay Mineral Compositions of Quaternary red Clay in Southern Anhui Province, Southeast China. Master's Thesis, Zhejiang Normal University, Zhejiang, China, 2012; pp. 1–53. (In Chinese).
60. Yang, S.Y.; Li, C.X.; Cai, J.G. Geochemical compositions of core sediments in eastern China: Implication for Late Cenozoic Palaeoenvironmental changes. *Palaeogeogr. Palaeoclimatol. Palaeoecol.* **2006**, *229*, 287–302. [CrossRef]
61. Nesbitt, H.W.; Markovics, G. Weathering of granodioritic crust, long-term storage of elements in weathering profiles, and petrogenesis of siliciclastic sediments. *Geochim. Cosmochim. Acta* **1997**, *61*, 1653–1670. [CrossRef]
62. Wei, G.J.; Liu, Y.; Li, X.H.; Shao, L.; Fang, D.Y. Major and trace element variations of the sediments at ODP Site 1144, South China Sea, during the last 230 ka and their paleoclimate implications. *Palaeogeogr. Palaeoclimatol. Palaeoecol.* **2004**, *212*, 331–334. [CrossRef]
63. Tang, Y.J.; Jia, J.Y.; Xie, X.D. Environment significance of clay minerals. *Earth Sci. Front.* **2002**, *9*, 337–344. (In Chinese)
64. Bain, D.C. The weathering of chloritic minerals in some Scottish soils. *Eur. J. Soil Sci.* **1977**, *28*, 144–164. [CrossRef]
65. Sun, Q.F.; Colin, C.; Chen, F.H.; Zhang, J.W. A discussion on the factors affecting Formation and quantity of clay minerals in climatic and environmental researches. *Acta Petrol. Mineral.* **2011**, *30*, 291–300. (In Chinese)
66. Gao, Y.; Gao, Y.; Ibarra, D.E.; Du, X.; Dong, T.; Liu, Z.; Wang, C. Clay mineralogical evidence for mid-latitude terrestrial climate change from the latest Cretaceous through the earliest Paleogene in the Songliao Basin, NE China. *Cretac. Res.* **2021**, *124*, 104827. [CrossRef]
67. Chamley, H. *Clay Sedimentology*; Springer: Berlin/Heidelberg, Germany, 1989.
68. Zhang, H.Y.; Yang, W.T. Research Status of Deep-time Paleoclimate Analysis Methods for Terrestrial Pulveryte and Paleosols. *Acta Sedimentol. Sin.* **2023**, *41*, 333–348. (In Chinese)
69. Song, E. Clay Mineralogy of the Gerze Sediments and Pal- Aeoclimatic Evolution in the Central Qinghai-Tibetan Plateau. Ph.D. Thesis, China University of Geosciences, Wuhan, China, 2014; pp. 1–116. (In Chinese).
70. Zhang, Z.B.; Xu, Y.; Miao, Y.J.; Wang, W.F.; Zhao, D.F.; Chen, D.L. Provenance and Sedimentary Environment of Paleogene Gongjue Formation in Qamdo Basin. *Acta Sediment. Sin.* **2022**, *40*, 1561–1581. (In Chinese)
71. Jones, D.S.; Fike, D.A. Dynamic sulfur and carbon cycling through the End-Ordovician extinction revealed by paired sulfate-pyrite δ^{34}S. *Earth Planet. Sci. Lett.* **2013**, *363*, 144–155. [CrossRef]
72. Bartlett, R.; Elrick, M.; Wheeley, J.R.; Polyak, V.; Desrochers, A.; Asmerom, Y. Abrupt global-ocean anoxia during the Late Ordovician–Early Silurian detected using uranium isotopes of marine carbonates. *Proc. Natl. Acad. Sci. USA* **2018**, *115*, 5896–5901. [CrossRef]
73. Jing, X.Q.; Yang, Z.Y.; Ross, N.M.; Tong, Y.B.; Zhu, M.; Wan, B. Ordovician–Silurian true polar wander as a mechanism for severe glaciation and mass extinction. *Nat. Commun.* **2022**, *13*, 7941. [CrossRef]
74. Qiu, Z.; Lu, B.; Chen, Z.H.; Zhang, R.; Dong, D.Z.; Wang, H.Y.; Qiu, J.L. Discussion of the Relationship between Volcanic Ash Layers and Organic Enrichment of Black Shale: A case study of the Wufeng-Longmaxi gas shales in the Sichuan Basin. *Acta Sedimentol. Sin.* **2019**, *37*, 1296–1308. (In Chinese)
75. Zhang, Z.; Guo, Y.; Zhao, D.; Zhang, J.; Zeng, C.; Li, Y. Control Model of Organic Shale Enrichment by TerrigenousWeathering inWufeng Formation–LongmaxiFormation, Southeast Sichuan, China. *Minerals* **2023**, *13*, 761. [CrossRef]
76. Lu, X.; Kendall, B.; Stein, H.J.; Li, C.; Hannah, J.L.; Gordon, G.W.; Ebbestad, J.O.R. Marine redox conditions during deposition of Late Ordovician and Early Silurian organic-rich mudrocks in the Siljan ring district, central Sweden. *Chem. Geol.* **2017**, *457*, 75–94. [CrossRef]
77. Kampschulte, A.; Strauss, H. The sulfur isotopic evolution of Phanerozoic seawater based on the analysis of structurally substituted sulfate in carbonates. *Chem. Geol.* **2004**, *204*, 255–286. [CrossRef]

78. Present, T.M.; Paris, G.; Burke, A.; Fischer, W.W.; Adkins, J.F. Large Carbonate Associated Sulfate isotopic variability between brachiopods, micrite, and other sedimentary components in Late Ordovician strata. *Earth Planet. Sci. Lett.* **2015**, *432*, 187–198. [CrossRef]
79. Goldman, D.; Sadler, P.M.; Leslie, S.A. *Chapter 20—The Ordovician Period*; Elsevier: Amsterdam, The Netherlands, 2020; pp. 489–523.79.